Journal of Photochemistry and Photobiology C: Photochemistry Reviews 18 (2014) 50–70

Contents lists available at ScienceDirect

Journal of Photochemistry and Photobiology C: Photochemistry Reviews

journal homepage: www.elsevier.com/locate/jphotochemrev

Invited review

Synthesis and photoreactivity of α-diketone-type precursors of acenes and their use in organic-device fabrication

Mitsuharu Suzuki[a,*], Tatsuya Aotake[a], Yuji Yamaguchi[b], Nao Noguchi[c], Haruyuki Nakano[c,*], Ken-ichi Nakayama[b,d,*], Hiroko Yamada[a,d,**]

[a] Graduate School of Materials Science, Nara Institute of Science and Technology, Ikoma 630-0192, Japan
[b] Department of Electrical Devices, Graduate School of Science and Engineering, Yamagata University, Yonezawa 992-8510, Japan
[c] Department of Chemistry, Graduate School of Sciences, Kyushu University, Fukuoka 812-8581, Japan
[d] CREST, JST, Chiyoda-ku 102-0076, Japan

ARTICLE INFO

Article history:
Received 2 August 2013
Received in revised form 2 October 2013
Accepted 8 October 2013

Keywords:
Acenes
Pentacene
Decarbonylation
Photoprecursor method
Organic electronics
Solution processes

ABSTRACT

Acenes are highly promising p-type organic semiconductors, and have been the subject of intense studies. However, acenes are often low in solubility and stability, which poses major obstacles in the synthesis and processing of this class of compounds. In order to overcome the problem, a series of α-diketone-type acene precursors have been developed. These precursors are generally more soluble and stable than the corresponding acene compounds, and their quantitative conversion can be achieved simply by photoirradiation both in solution and in the solid state. Further, the irreversible photoinduced removal of the α-diketone unit can be used to alter the optoelectronic properties of fluorophores. This review overviews the synthesis and photochemical properties of α-diketone-type acene precursors, as well as their use as intermediates in preparation of large acenes or highly functionalized acene derivatives. Computational studies on the mechanism of α-diketone photolysis and the use of α-diketone derivatives in fabrication of organic devices are also summarized in this review.

Contents

Abbreviations: AFM, atomic force microscopy; BHJ, bulk heterojunction; CIS, configuration interaction singles; DBU, 1,8-diazabicyclo[5.4.0]undec-7-ene; DCB, *o*-dichlorobenzene; DIBAL, diisobutylaluminium hydride; DDQ, 2,3-dichloro-5,6-dicyanobenzoquinone; DFT, density functional theory; DMSO, dimethyl sulfoxide; EQE, external quantum efficiency; FET, field-effect transistor; FF, fill factor; HOMO, highest occupied molecular orbital; ICT, intramolecular charge-transfer; IR, infrared; LED, light-emitting diode; LUMO, lowest unoccupied molecular orbital; MD, molecular dynamics; MO, molecular orbital; NMO, *N*-methylmorpholine-*N*-oxide; NMR, nuclear magnetic resonance; OPV, organic photovoltaics; PCBM, [6,6]-phenyl-C_{61}-butyric acid methyl ester; PCE, photo-conversion efficiency; PES, potential energy surface; PMMA, poly(methyl methacrylate); RHF, restricted Hartree–Fock; TCB, trichlorobenzene; TD, time-dependent; TEMPO, 2,2,6,6-tetramethylpiperidine-1-oxyl; TFAA, trifluoroacetic anhydride; UV, ultraviolet,vis,visible; XRD, X-ray diffractometry.

* Corresponding authors.
** Corresponding author. Tel.: +81 743 72 6041; fax: +81 743 72 6042.
E-mail addresses: msuzuki@ms.naist.jp (M. Suzuki), nakano@chem.kyushu-univ.jp (H. Nakano), nakayama@yz.yamagata-u.ac.jp (K. Nakayama), hyamada@ms.naist.jp (H. Yamada).

1389-5567/$20.00 © 2013 Elsevier B.V. All rights reserved.
http://dx.doi.org/10.1016/j.jphotochemrev.2013.10.003

Mitsuharu Suzuki received his B.Eng. (2000) and M.Eng. (2002) in industrial chemistry from Kyoto University (Japan). After working in Mitsubishi Gas Chemical Company as a researcher, he moved to the United States and received his Ph.D. in chemistry from University of California, Los Angeles in 2011. He then worked as a postdoctoral fellow at the same institute and Lawrence Berkeley National Laboratory, before joining Nara Institute of Science and Technology (Japan) as an assistant professor in 2013. His current research focuses on the development of solution-processable molecular materials for organic electronics applications.

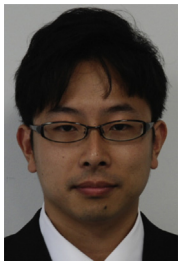

Tatsuya Aotake was born in 1987 in Kagawa, Japan. He received his M.Sc in 2011 from Ehime University under the direction of Professor Hidemitsu Uno. Currently, he is a Ph.D. student in the research group of Professor Hiroko Yamada at Nara Institute of Science and Technology. His research interest is organic synthetic chemistry for photofunctional materials.

Yuji Yamaguchi received his M.Sc. degree in 2008 and his Ph.D. in 2013 from Yamagata University. Now, he has been a JST-CREST Postdoctoral Research Fellow. His research interests include organic synthesis, material science in organic transistors and organic photovoltaic device.

Nao Noguchi received her master's degree in chemistry from Kyushu University in 2006. She then joined Pfizer and moved to Takeda Pharmaceuticals in 2009, where she is now a research scientist.

Haruyuki Nakano received his Ph.D. in chemistry in 1993 working under the direction of Professor Shigeki Kato at Kyoto University. He then joined the faculty of the University of Tokyo. In 2003, he moved to Kyushu University at Fukuoka, where he is now Professor of Theoretical Chemistry. His research interest includes the development of many-body electronic structure theory and its application to problems of broad chemical interest.

Ken-ichi Nakayama received his B. S. degree in Applied Chemistry in 1995, and his Ph.D. in 2000, from Osaka University (Japan) under the direction of Prof. Masaaki Yokoyama. He then became an Assistant Professor at Osaka University, and started his research on organic devices. In 2006, he moved to Yamagata University (Japan) as an Associate Professor, and he joined Prof. Junji Kido's group. He was also appointed as a researcher of Japan Science and Technology Agency (JST) in PRESTO project (2006–2010). His research interests include device engineering and material science in organic transistors and organic photovoltaic devices.

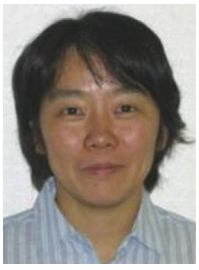

Hiroko Yamada received her Ph.D. degree (Science) in 1992 from Kyoto University. Since 2008, she was an associate professor at Ehime University, then moved to Nara Institute Science and Technology in 2011. She was promoted to a full professor at NAIST in 2012. From 2007 to 2010, she was a researcher of PRESTO, Japan Science and Technology Agency (JST), and then a group leader of CREST project (2010–2015), JST, on "Construction of organic thin-film solar cells with innovative solution-processible organic materials". Her current research focuses on the development of functional organic materials including solution-processable molecular materials for organic electronics applications, large acenes and porphyrinoid compounds.

1. Introduction

Solution-processable organic semiconductors hold much promise as active components in optoelectronic devices owing to their potential for permitting large-scale fabrication of thin, flexible, and lightweight devices based on simple processing techniques [1–21]. Many research laboratories have devoted considerable efforts towards this end, and the progress during the past two decades is significant as can be manifested by, for example, the current use of organic light-emitting diode displays in commercial devices. However, the commercialization of organic devices is still limited, and most other organic devices such as organic photovoltaic cells and organic field-effect transistors remain elusive in the market. Further advance in both material design and device-fabrication process is required before various types of organic devices become widely available so that society can fully appreciate their great advantages.

Acenes, which can be described as linearly fused benzene rings (Fig. 1), have been the subject of intense studies in the organic semiconductor research [22–25]. For example, unsubstituted pentacene (**1**) is one of the routinely employed p-type semiconductors, which shows carrier mobilities of over 5 $cm^2 V^{-1} s^{-1}$ [26]—among the highest charge carrier mobilities obtained with organic materials so far. However, unsubstituted acenes are not necessarily well-suited for commercial applications largely because of their low solubility and stability; pentacene and larger acenes are hardly soluble in common organic solvents and easily oxidized in air to form the corresponding quinones [22,23,27]. These shortcomings keep the preparation and processing of unsubstituted acenes from being scalable and cost-effective. Accordingly, one of the main subjects in acene chemistry is to develop stable and solution-processable

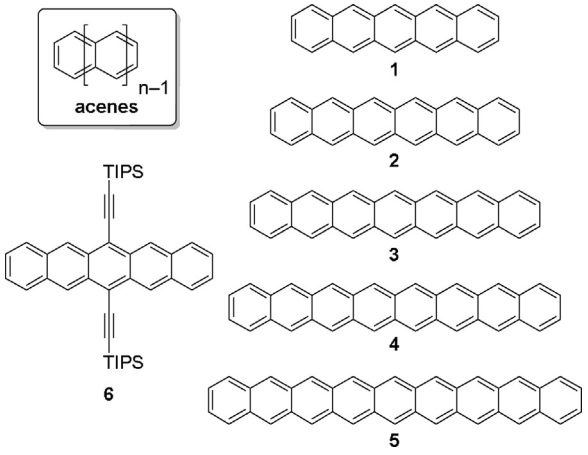

Fig. 1. General structure of acenes (top-left), structures of acene series from pentacene (**1**) to nonacene (**5**) and the soluble derivative of pentacene developed by Anthony et al. (**6**).

derivatives without adversely affecting their intrinsic useful properties as organic semiconductors.

A milestone in the development of device-oriented acene derivatives is the synthesis of 6,13-bis(triisopropylsilylethynyl) pentacene (**6**, Fig. 1) reported by Anthony et al. in 2001 [28]. Derivative **6** is soluble in common organic solvents and stable under ambient conditions allowing not only deposition via simple solution-based techniques, but also easy purification after synthesis. In addition, the compound adopts a "brickwork arrangement" in the crystalline state, in which the face-to-face π contact between pentacene units extends two dimensionally. This packing motif is favorable for charge carrier transportation; indeed, Bao and coworkers demonstrated in their recent report that the hole mobility in solution-processed FET devices based on compound **6** can be as high as 11 $cm^2 V^{-1} s^{-1}$ [29]. This value is higher than those observed for the parent pentacene or for amorphous silicon (typically in the order of 1 $cm^2 V^{-1} s^{-1}$) [30]. Following the development of compound **6**, many substituted pentacenes and larger acenes have been evaluated as summarized in previous reviews [22–24].

Another approach to achieve both solution processability and high device performance with acenes is to introduce solubilizing groups that are cleanly removable after deposition [31]. A pioneering work along this line was reported by Müllen and coworkers in 1996 [32]. The authors developed a tetrachlorobenzene–pentacene adduct (**7**, Fig. 2), which can be deposited as a solution and converted to the parent pentacene (**1**) in the film via thermally induced retro Diels–Alder reaction at 180 °C. Charge carrier mobilities as high as 9×10^{-3} $cm^2 V^{-1} s^{-1}$ were observed in the resulting films. Following this, other thermolabile derivatives of pentacene (**8**–**14**) were proposed by different groups [33–40], and hole mobilities of up to 0.89 $cm^2 V^{-1} s^{-1}$ [33] were achieved in the resulting pentacene films. In some cases, the thermolytic conversion to pentacene proceeded at temperatures as low as 120–130 °C [33,35,37], suggesting the potential compatibility of this method with plastic substrates.

Photolysis, instead of thermolysis, can be also used for the post-deposition conversion of soluble precursors to insoluble acenes. (This methodology is called 'photoprecursor method' in the followings of this review.) Since photolysis can be performed at ambient temperature or lower, its scope for applicable substrates would be much wider compared to that of thermolysis. In addition, the photoprecursor method may permit light pattering of the active layer by employing the already well-established photolithography techniques. These advantages motivated the development

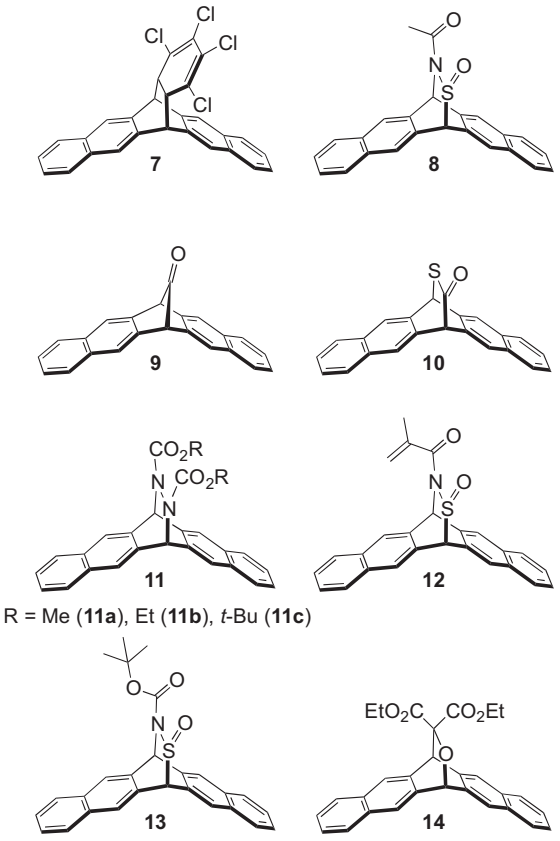

Fig. 2. Structures of the known thermo-convertible precursors of pentacene [32–36,39,41].

of photoconvertible acene precursors. In this context, Chow and coworkers prepared monoketone derivatives of acenes including compound **9**, which can be transformed to the parent acenes both by thermolysis and photolysis [41–47]. This review specifically focuses on another class of photo-convertible precursors of acenes; i.e., α-diketone-type precursors. The following sections summarize the synthesis and photochemical properties of the α-diketone-type precursors reported so far. Described also are computational investigation on the mechanism of their photoconversion and their use in the fabrication of acene-based organic devices.

2. Synthesis and photoreactivity of α-diketone-type precursors of acenes

2.1. Background chemistry

In 1968, Bryce-Smith and Gilbert reported the photolytic decarbonylation of α-diketone **15** to form tetrachloro-*o*-terphenyl **21** both in solution and in the crystalline state under visible light (Scheme 1) [48]. While the thermal decarbonylation of monoketone compounds was already well-documented by then [49], the photoinduced decarbonylation of α-diketones had been unknown until this report. Almost at the same time, Strating and coworkers reported that α-diketones **16**–**19** underwent smooth photolysis to form the corresponding aromatic compounds (Scheme 1) [50]. The reactions were performed in benzene solutions using a high-pressure mercury lamp to yield compound **22**–**25** in quantitative, 97%, 95%, and 43% yield, respectively. They also found that compound **20** could undergo photoinduced decarbonylation to form cyclohexadiene **26**, indicating that aromatic stabilization in the product would not necessarily be the requirement for this type of photolysis. A while later, Pyle et al. applied this method to the

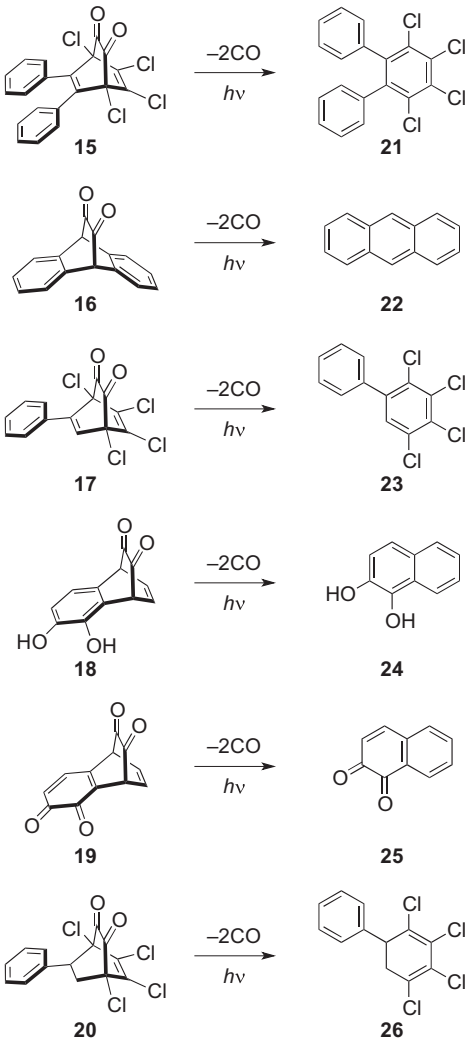

Scheme 1. Photoinduced decarbonylation of α-diketones reported by Bryce-Smith and Gilbert [48], and Strating et al. [50].

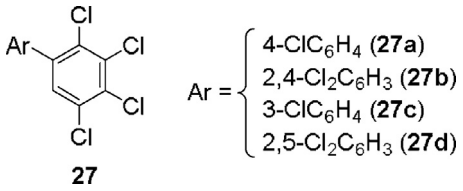

Fig. 3. Unsymmetrically chlorinated biphenyls synthesized by Pyle et al. via photolytic decarbonylation [51].

synthesis of unsymmetrically substituted chlorobiphenyls **23** and **27** with the aim of using these differently chlorinated biphenyls in toxicological studies (Scheme 1 and Fig. 3) [51]. The cleanliness of the photoinduced decarbonylation allowed easy workup and isolation to provide good overall yields and high purity of the final products, which is critical in the toxicological studies. A different group also applied this method to prepare highly substituted derivatives of indene and benzene (Scheme 2) [52]. Although the synthetic application of the photolytic decarbonylation of α-diketones has been rather limited, the above examples clearly show its usefulness in the synthesis of highly functionalized small acenes and other related classes of compounds. The mechanism of this decarbonylation has been under investigation for long since immediately after the discovery of the reaction [50,53–55], which will be described separately in Section 3.

2.2. α-Diketone-type precursors of unsubstituted acenes

2.2.1. Precursors to pentacene

The use of α-diketone derivatives as soluble precursors of acenes was pioneered by Ono, Uno, Yamada and coworkers [56–58]. Synthesis of the symmetric α-diketone precursor of pentacene (**37**, Scheme 3) was started with the double coupling of tetramethylene **32** and benzyne, followed by oxidative aromatization by the action of 2,3-dichloro-5,6-dicyanobenzoquinone (DDQ) to form intermediate **33**. Dihydroxylation of the etheno bridge with OsO_4 provided diol **36**, which was then subjected to the Swern oxidation conditions to form the target α-diketone **37** (Scheme 3, route A). Alternatively, **37** could be also synthesized from the parent

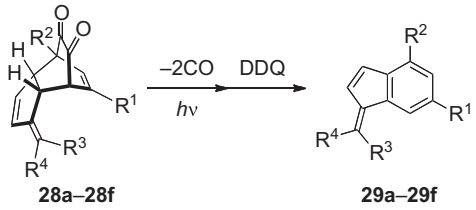

	R1	R2	R3	R4
a	*t*-Bu	*t*-Bu	Ph	Ph
b	*t*-Bu	H	Ph	Ph
c	H	OCH_3	Ph	Ph
d	*t*-Bu	*t*-Bu	H	Ph
e	*t*-Bu	H	H	Ph
f	*t*-Bu	*t*-Bu	H	4-$MeOC_6H_4$
g	*t*-Bu	*t*-Bu	CH_3	Ph
e	*t*-Bu	H	CH_3	Ph

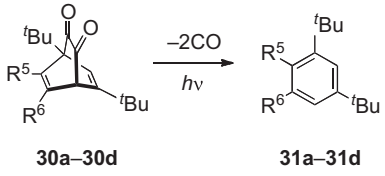

	R5	R6
a	CO_2Me	CO_2Me
b	H	CH_2OH
c	Ph	H
d	H	Ph

Scheme 2. Synthesis of highly functionalized indene and benzene derivatives via photolysis of α-diketones [52].

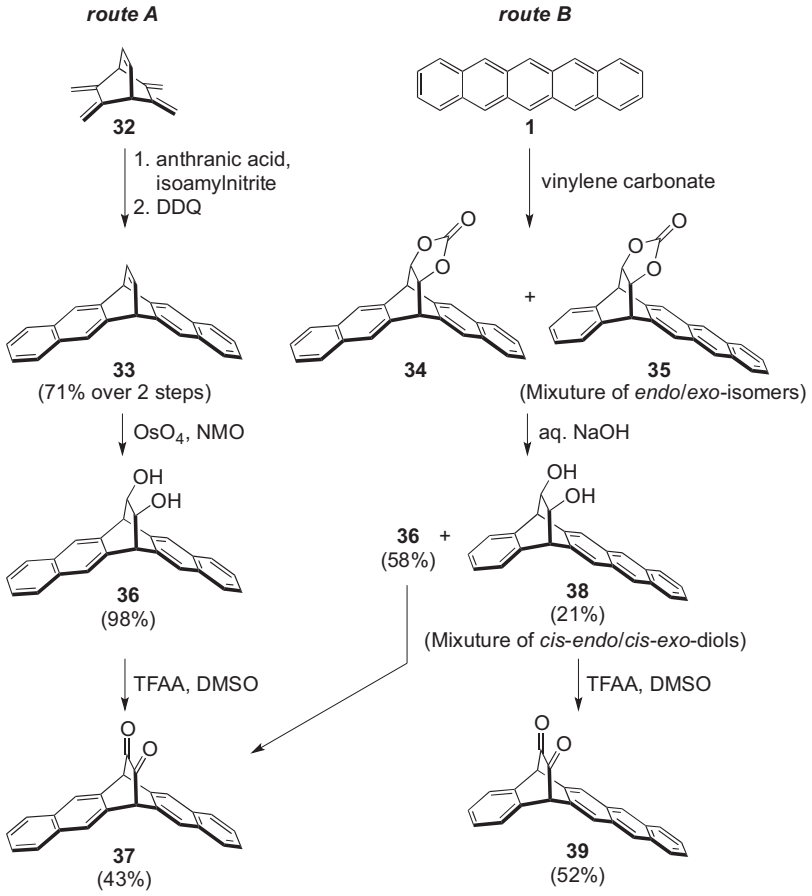

Scheme 3. Synthesis of α-diketone-type pentacene precursors **37** and **39** [56–58].

pentacene (**1**) via the Diels–Alder addition with vinylene carbonate followed by hydrolysis under basic conditions (route B). In the latter route, the Diels–Alder addition afforded both the 6,13- and 5,14-isomers (**34** and **35**), which were separated after hydrolysis simply by silica gel column chromatography to provide **36** and **38** with the isolation yields of 58% and 21%, respectively. Here, the yield of compound **36** could be improved to 88% by employing the reaction conditions optimized for the formation of the 6,13-adduct [57]. The diketone precursors thus obtained are considerably more soluble in organic solvents compared to the parent pentacene (**1**): the solubility of **37** and **39** in toluene at 25 °C are 2.3 and 0.44 mg mL^{-1}, respectively, while **1** is essentially insoluble under the same conditions.

The n–π* absorptions associated with the α-diketone moieties of **37** and **39** were observed at 466 ($\varepsilon = 1.22 \times 10^3$ M^{-1} cm^{-1}) and 464 nm (1.58×10^3 M^{-1} cm^{-1}), respectively (Fig. 4). The π–π* absorption peaks arising from the naphthalene units of **37** were observed at 329 (4.23×10^3 M^{-1} cm^{-1}) and 315 (4.05×10^3 M^{-1} cm^{-1}), while those from the anthracene unit in **39** were at 367 (4.20×10^3 M^{-1} cm^{-1}), 349 (5.40×10^3 M^{-1} cm^{-1}), and 333 nm (5.49×10^3 M^{-1} cm^{-1}). A broad peak was additionally observed at 386 nm (2.98×10^3 M^{-1} cm^{-1}) for **39**, which was ascribed to the intramolecular charge-transfer (ICT) from the anthracene moiety to the α-diketone unit based on the solvent dependence of photoabsorption behavior and DFT calculations [58].

The photolysis of α-diketones **37** and **39** to form pentacene (**1**) proceeded smoothly in toluene with quantum yields (Φ_r) of 1.4 ± 0.3% and 2.3 ± 0.3%, respectively, when they were irradiated at 468 nm corresponding to the n–π* absorption of α-diketone unit (Fig. 5). In the case of **39**, the photolysis could be also induced by 405-nm light, which corresponds to the ICT absorption, with a Φ_r of

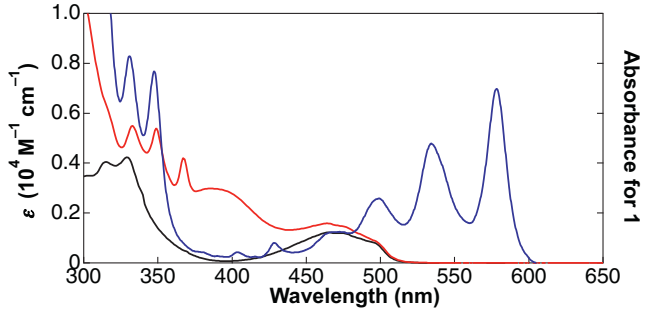

Fig. 4. UV–vis absorption spectra of **1** (blue) and its α-diketone-type precursors **37** (black) and **39** (red) in toluene [58].

2.4 ± 0.3%. On the other hand, the reaction efficiency was considerably lower in acetonitrile: the observed Φ_r values were 0.80 ± 0.12% and 0.28 ± 0.10% for **37** and **39**, respectively, under irradiation at 468 nm. The reaction was similarly inefficient when compound **39** was irradiated at 405 nm in acetonitrile ($\Phi_r = 0.33 \pm 0.13\%$). The authors assumed that the lower Φ_r values in the more polar solvent, acetonitrile, would be due to efficient electron transfer in the singlet excited state to form a charge-separate species which then decays to the ground state mainly via a nonproductive, radiationless pathway. In the less polar solvent, toluene in this case, the charge-separate state would experience less stabilization, thereby being located higher in energy. Consequently, the photoreaction pathway becomes more favorable, leading to the higher Φ_r values.

The photoconversion of α-diketone **37** to pentacene (**1**) was also conducted in a thin film under exclusion of oxygen. The conversion was monitored through change in photoabsorption—the n–π*

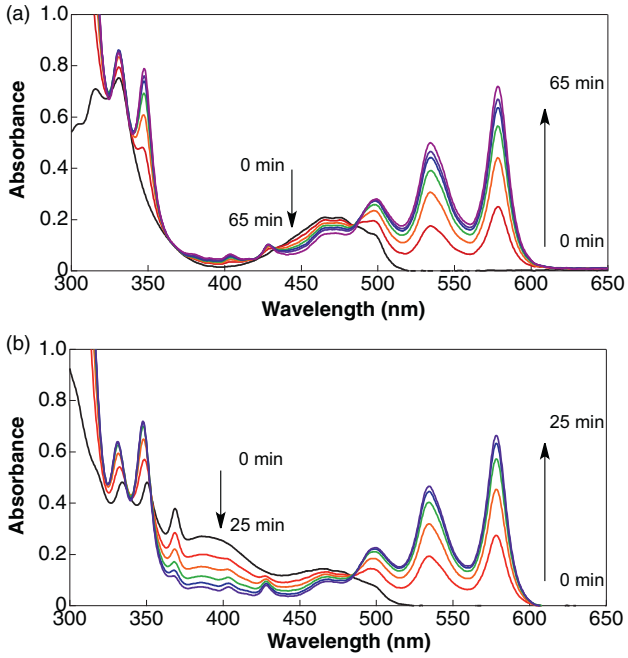

Fig. 5. Change in absorption spectra during the photolysis of α-diketone-type pentacene precursors **37** (a) and **39** (b) in toluene [58].

absorption at 470 nm disappeared upon photoirradiation, while new peaks emerged at 585, 627, and 648 nm in good agreement with the reported data for deposited samples of **1** [59]. The quantitative conversion of **37** was confirmed by absence of the carbonyl stretch in the IR spectrum of the resulting film. Unsymmetrical isomer **39** also underwent the photoinduced decarbonylation in a thin film, as indicated by change in photoabsorption. In this case, however, the solid-state UV–vis spectrum of pre-reaction sample showed only very broad, featureless absorption without any well-structured peaks. The authors supposed that the significant broadening of photoabsorption peaks would be due to the strong π–π interaction between the molecules of **39** in the film. Indeed, compound **39** has higher crystallinity and tighter crystal packing compared to symmetric isomer **37**, even though the overall crystal-packing motifs are essentially the same for those two compounds. The absorption spectrum of post-reaction film of **39** was also relatively featureless, but characteristic peaks for the expected product **1** were observed at 560 and 610 nm.

2.2.2. Precursors to larger acenes

While the parent pentacene (**1**) is widely available from commercial sources, larger acenes had been elusive even in research laboratories until very recently when the photoprecursor method was employed for their synthesis. Neckers et al. reported the synthesis of α-diketones **44** and **45**, which were photolytically converted to hexacene (**2**) and heptacene (**3**), respectively (Scheme 4) [60,61]. The required carbon frameworks were constructed by sequential coupling of tetramethylene **32** and the corresponding benzyne species. Similarly to the synthesis of pentacene precursors **37** and **39**, the α-diketone moiety was introduced via the two-step oxidation of the etheno bridge. The overall yield was 27% for **44**, and 18% for **45**.

The n–π* transition of α-diketone moiety was observed around 465 nm for both **44** and **45**, which is at essentially the same position as the corresponding peaks for the anthracene precursor **16** or pentacene precursors **37** and **39**. The π–π* transitions of **44** appeared at 327, 345, and 367 nm, while those of **45** were at 347 and 368 nm. Irradiation of a toluene solution of **44** at 395 ± 25 nm induced decarbonylation to afford hexacene (**2**), which could be monitored by change in UV–vis absorption. However, the product was highly unstable and quickly converted to the corresponding dimeric and oxidized species under the reaction conditions (concentration $<10^{-4}$ M), preventing detailed study of **2**. On the other hand, **2** could be kinetically stabilized in a matrix of poly(methyl methacrylate) (PMMA). The authors prepared a thin film (ca. 0.5 mm thickness) of PMMA containing 3.5×10^{-3} M of α-diketone **44**. Reaction monitoring through photoabsorption spectra indicated the smooth formation of **2** in the film, which was further confirmed by mass spectroscopy. The product could be retained in the polymer matrix overnight under ambient conditions [60]. Detection and characterization of heptacene (**3**) were even more challenging. The formation of **3** could not be observed directly in the photolysis of **45** in solution indicating its extremely unstable nature, and accordingly only the polymer matrix method allowed unambiguous characterization of the product. Irradiation of **45** dispersed in a thin film of PMMA (3.0×10^{-3} M, 0.5 mm thickness) resulted the appearance of new structured absorption ranging from 600 to 825 nm with the maximum around 760 nm, which was assigned to the π–π* transition of **3**. The formation of **3** was also confirmed by mass spectroscopy, and the product was stable up to 4 h in the PMMA matrix. Following these synthetic achievements, the same group investigated the properties of **3** in the solidified inert-gas matrix at 10 K [61,62]. In a separate report, the same team applied the acene-containing polymer matrix system to evaluate the oxygen permeability of polymers [63].

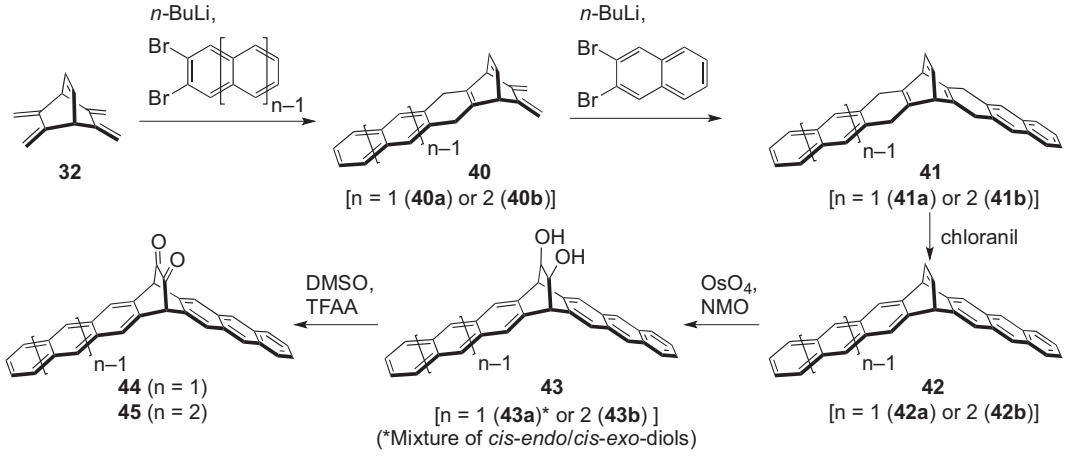

Scheme 4. Synthesis of α-diketone-type precursors **44** and **45** by Neckers and coworkers [60,61].

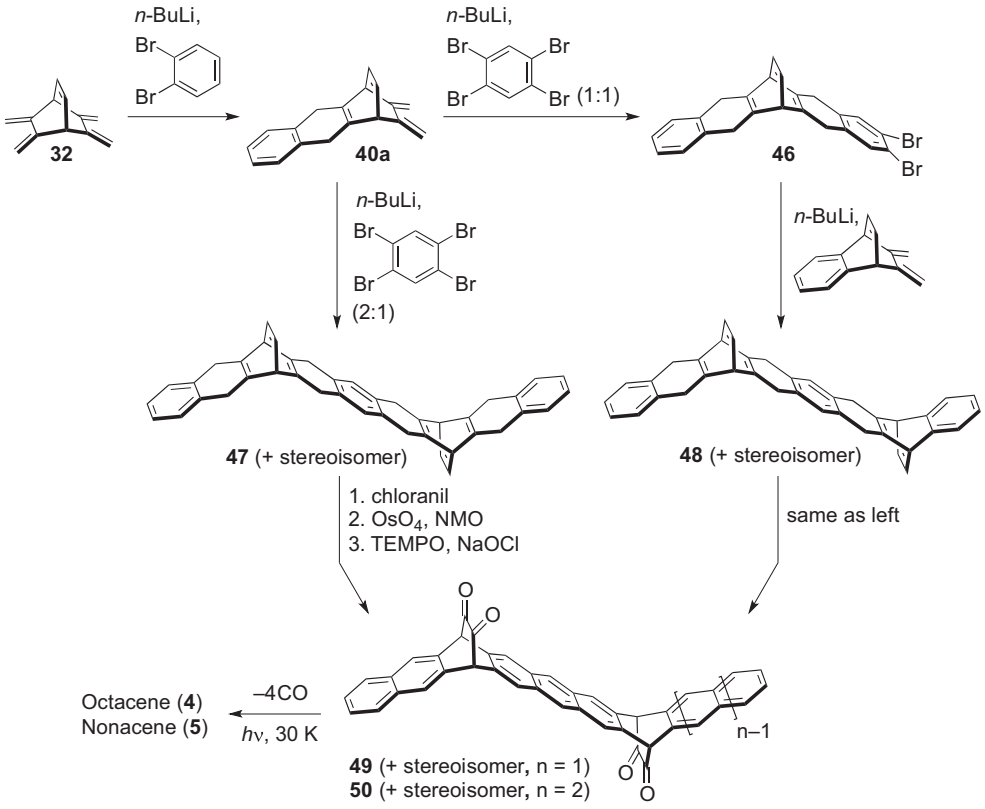

Scheme 5. Synthesis of photoprecursors **49** and **50** by Tönshoff and Bettinger [64].

More recently, Tönshoff and Bettinger reported the preparation of octacene (**4**) and nonacene (**5**) by photolysis of the corresponding α-diketone-type precursors **49** and **50**, respectively (Scheme 5) [64]. These photoprecursors were designed not to contain subunits longer than anthracene for the sake of ensuring stability and solubility, and thus two α-diketone bridges per molecule were introduced. Another difference in this synthesis from the previous examples is that a radical-based method was employed for the final oxidation step. Oxidation under the Swern conditions or by *o*-iodoxybenzoic acid turned out to be ineffective in this specific case, and instead the combination of 2,2,6,6-tetramethylpiperidine-1-oxyl and NaOCl was used. The photolysis of **50** to **5** proceeded in two steps via intermediate **51** under the employed reaction conditions (Scheme 6). Upon the irradiation of visible light (>360 nm), only one of the two α-diketone bridges was extruded to generate a hexacene subunit, while the complete photolysis was achieved by the irradiation of UV light at 305–320 nm. Irradiation at an even shorter wavelength of 185 nm induced photo-ionization. The shorter analogue **49** and its stereoisomer showed similar photoreactivity.

The examples described above clearly demonstrate the power of photoprecursor approach in the synthesis of large acenes, which provides an efficient access to this interesting class of compounds and enables investigation of their properties. Further exploration for better processing techniques or for kinetically stabilized derivatives would allow the practical use of acenes in devices. Along these lines, the recent beautiful work by Chow and coworkers is of special interest, where the authors succeeded in the preparation of single-crystalline samples of hexacene (**2**) from a monoketone-type precursor **52** via thermolytic decarbonylation (Scheme 7) [45]. The FET devices based on thus obtained single crystals showed hole mobilities of up to 4.28 $cm^2 V^{-1} s^{-1}$. The same group also reported monoketone-type precursors **9**, **53**, and **54** which are both

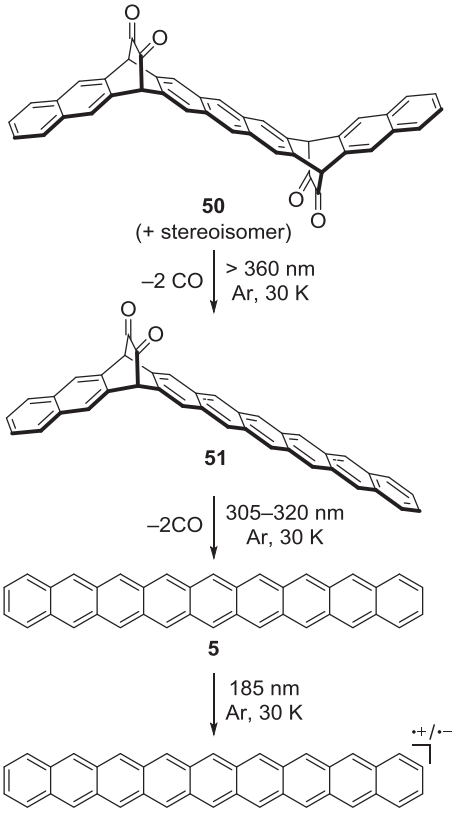

Scheme 6. Photochemical synthesis of nonacene (**5**) and its photoinduced ionization in a solid argon matrix at 30 K [64].

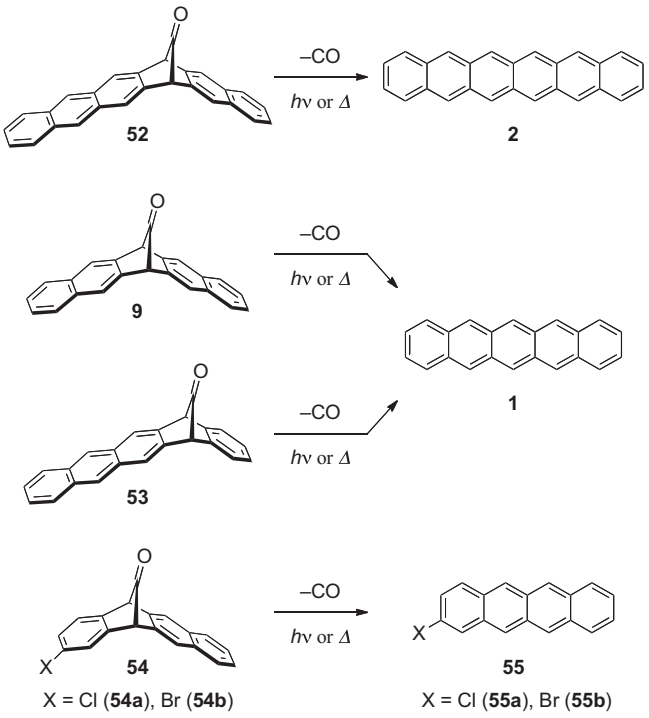

Scheme 7. Examples of monoketone-type precursors of acenes reported by Chow and coworkers [41,42,44–46].

thermally and photochemically convertible to the corresponding acenes (Scheme 7).

2.3. α-Diketone-type precursors of substituted acenes

2.3.1. Synthesis of end-substituted pentacenes via α-diketone-type precursors

As described in Section 1, the use of parent acenes in practical applications has been largely hampered by their instability and insolubility. Various derivatives of acenes, especially of pentacene (**1**), have been synthesized in order to improve the processability as well as to tune the optoelectronic properties and solid-state organization. A classical synthetic approach to functionalized acenes is the nucleophilic addition of organolithium reagents or organomagnesium halides to the corresponding quinone derivatives followed by reductive aromatization [65,66]. This approach has been employed for a wide variety of 6,13-substituted pentacenes including the 6,13-bis(triisopropylsilylethynyl)pentacene (**6**) and 6,13-connected oligomeric pentacene derivatives [22,24]. Another approach is the homologation method [67–71], which allows facile access to end-functionalized derivatives. Alternatively, one can employ the α-diketone route, where an α-diketone derivative is first synthesized via the addition of tetramethylene **32** and required benzyne compounds, followed by the oxidation of etheno bridge. The resulting α-diketone is then subjected to decarbonylation to form the target pentacene derivative. Similarly to the homologation method, this approach is suitable for the synthesis of end-substituted pentacenes, because derivatization can be achieved by simply changing the benzyne unit to be coupled with **32**. This latter approach is described in more detail in this section.

In 2005, Yamada et al. reported the synthesis of 2,9- and 2,10-dibromopentacenes (**59**) via the photo-decarbonylation of the corresponding α-diketone-type precursors (Scheme 8) [57]. The authors prepared a mixture of 2,9- and 2,10-dibromo-6,13-ethanopentacenes (**57**) from 2-amino-5-bromobenzoic acid (**56**) and tetramethylene **32**. Sequential oxidation of **57** led to the formation of α-diketone **58**. Here, the 2,9- and 2,10-isomers were hard to separate, and the product was isolated as a mixture of the two regioisomers. The photoconversion of **58** was performed in a degassed toluene solution by using a super-high-pressure mercury lamp (500 W) through UV and IR cut-off filters. A purple precipitate appeared upon photoirradiation, which was identified as the corresponding isomeric mixture of dibromopentacenes (**59**) based on mass spectroscopic analysis. The isolation yield of this photolysis was 79%.

Neckers and coworkers reported photochemical syntheses of 2,3-di- and 2,3,9,10-tetrasubstituted pentacenes via the photolysis of α-diketone-type precursors (Scheme 9) [72,73]. The synthesis of tetrasubstituted pentacenes **66a**–**66c** was started with the double Diels–Alder addition between dibromobenzyne **61** and tetramethylene **32**. On the other hand, the carbon framework of disubstituted derivatives **71a** and **71b** was constructed by stepwise Diels–Alder reactions in which dibromo- and unsubstituted benzynes were sequentially reacted with **32**. After oxidative aromatization and introduction of different aryl groups by Suzuki–Miyaura coupling, the etheno bridge was oxidized to α-diketone in two steps. The photoinduced decarbonylation of thus obtained precursors proceeded smoothly to provide the target substituted pentacenes. In addition, 2,3,9,10-tetrabromopentacene (**72**) was obtained by employing the same strategy.

These substituted pentacenes are generally more soluble compared to the parent pentacene (**1**), allowing full monitoring of the photoinduced decarbonylation process in solution without precipitation of the product over the course of the reaction. Indeed, the authors were able to monitor the photoconversion of **70a** by solution NMR, which clearly showed that the formation of pentacene **71a** is essentially quantitative without forming any by-products [72]. The formation of **71a** was further confirmed by mass spectrometry and photoabsorption spectroscopy. Those substituted pentacenes are highly stable under inert atmosphere: the

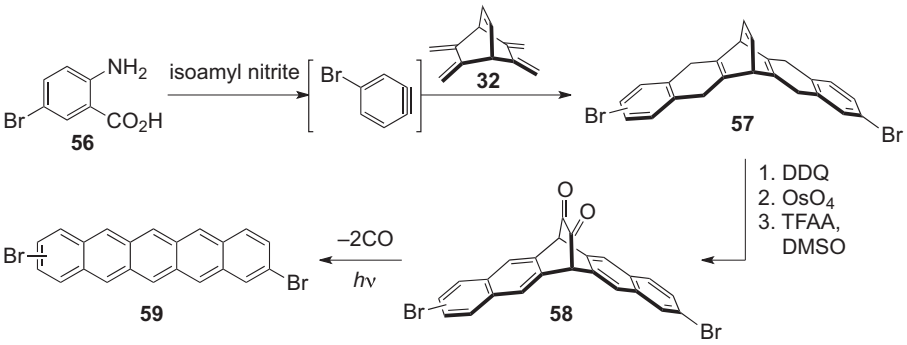

Scheme 8. Synthesis of dibromopentacenes by Yamada et al. [57]. The product was obtained as a mixture of 2,9- and 2,10-isomers.

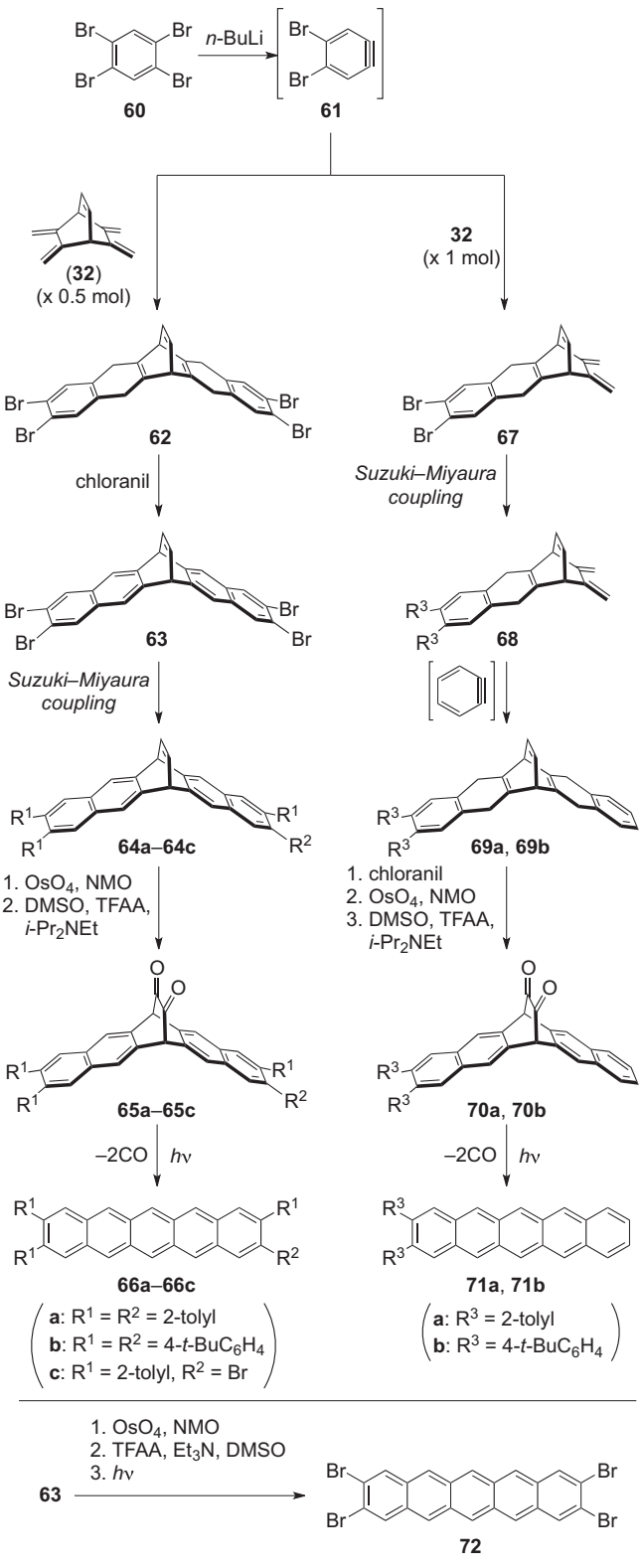

Scheme 9. Synthesis of 2,3-di- and 2,3,9,10-tetrasubstituted pentacenes by Neckers and coworkers [72,73].

converted pentacenes survived in solution for 1 month without showing any sign of dimerization or oxidation.

In 2009, Lin et al. reported the homologation synthesis of end-substituted acenes, wherein an [n]acene-*ortho*-dicarbaldehyde is converted to the corresponding [n+1]acene-*ortho*-dicarboxylate in one-pot (Scheme 10a) [74]. The dicarboxylate product can be transformed to dicarbaldehyde via a routine reduction–oxidation protocol, and then subjected to another iteration of elongation. In addition, dicyanoacenes can be obtained in the same fashion by employing fumaronitrile as a coupling partner. The authors successfully combined this strategy with the α-diketone approach to obtain tetraethyl 2,3,9,10-pentacenetetracarboxylate (**77**, Scheme 10b), in which the bidirectional elongation of tetracarbaldehyde **74** to form **75** was followed by the oxidation of etheno bridge to generate α-diketone **76**. The photolysis of **76** to **77** proceeded in 70–80% yield. The bidirectional elongation also provided other etheno-bridged compounds **78**–**80** (Scheme 10c), indicating the usefulness of this strategy in synthesizing a variety of electron-deficient acenes.

Photochemical synthesis of 1,4,8,11-tetraaryl pentacenes **84a** and **84b** was reported by Yamada and coworkers (Scheme 11) [75]. The synthesis was started with the preparation of the required 3,6-diarylanthranilic acids (**82a** and **82b**) in six steps from commercially available anhydride **81**. Following the regular Diels–Alder/oxidation sequence, **82a** and **82b** were converted to the target α-diketone-type precursors **83a** and **83b**, both of which underwent smooth photoinduced decarbonylation to form **84a** and **84b**, respectively. Here again, the photolysis process could be monitored by ^{1}H NMR and UV–vis spectra to confirm quantitative conversion to the corresponding pentacene derivatives (Fig. 6).

Recently, Tönshoff and Bettinger employed the photoprecursor approach for synthesizing tetramethoxy pentacene **86a** and push–pull type pentacene derivatives **86b**–**86d** (Scheme 12) [76]. The synthesis of α-diketones **85a**–**85d** was achieved through a similar synthetic route as Scheme 9. The photolysis proceeded smoothly both in argon matrix at 10 K and in CH_2Cl_2 solution. Progress of the photolysis reactions was monitored through change in UV–vis absorption, which indicated clean decarbonylation associated with isosbestic points. The clean, efficient formation of these interesting derivatives would enable a systematic investigation of their solid-state packing and charge carrier transport behavior.

2.3.2. Combination with other chromophores

The photoinduced decarbonylation is more than just a convenient synthetic means for preparing acenes and their derivatives. The drastic change in electronic structure associated with the decarbonylative aromatization is highly interesting in that it can irreversibly alter the (opto)electronic properties of a compound. For example, Aotake et al. showed that nonfluorescent α-diketone derivatives **90a** and **90b** could be quantitatively converted to highly fluorescent anthracene–pyrene dyads **91a** and **91b** via the photoinduced decarbonylation (Scheme 13) [77]. Aryl-substituted pyrenes are generally highly fluorescent [78–80], and both **91a** and **91b** are not exceptional: the observed fluorescent quantum yields in solution were 0.86 or higher, with the maximum of 0.99 observed for **91a** in benzonitrile. On the other hand, the α-diketone derivatives are not fluorescent owing to the quenching of pyrene excited state by the α-diketone moiety. The authors also demonstrated that photoconversion of these α-diketones could proceed in poly(methyl methacrylate) (PMMA) films, allowing photo-patterning as shown in Fig. 7. The α-diketone derivatives **90a** and **90b** were synthesized from 2-bromoanthracene **87** in four steps (Scheme 13).

Aotake et al. also designed masked tetracene derivatives **95a** and **95b** based on the same concept (Scheme 14) [81]. In this case again, the α-diketone derivatives are barely fluorescent, while decarbonylation products **94a** and **94b** are highly fluorescent. Synthesis of **95a** and **95b** was started with nucleophilic arylation of a known tetracenequinone **92**, followed by aromatization and Diels–Alder addition with vinylene carbonate. The target α-diketone derivatives were obtained after the routine hydrolysis and Swern oxidation sequence. The fluorescent quantum yields observed for **95a** and **95b** in toluene were 0.016 and 0.017,

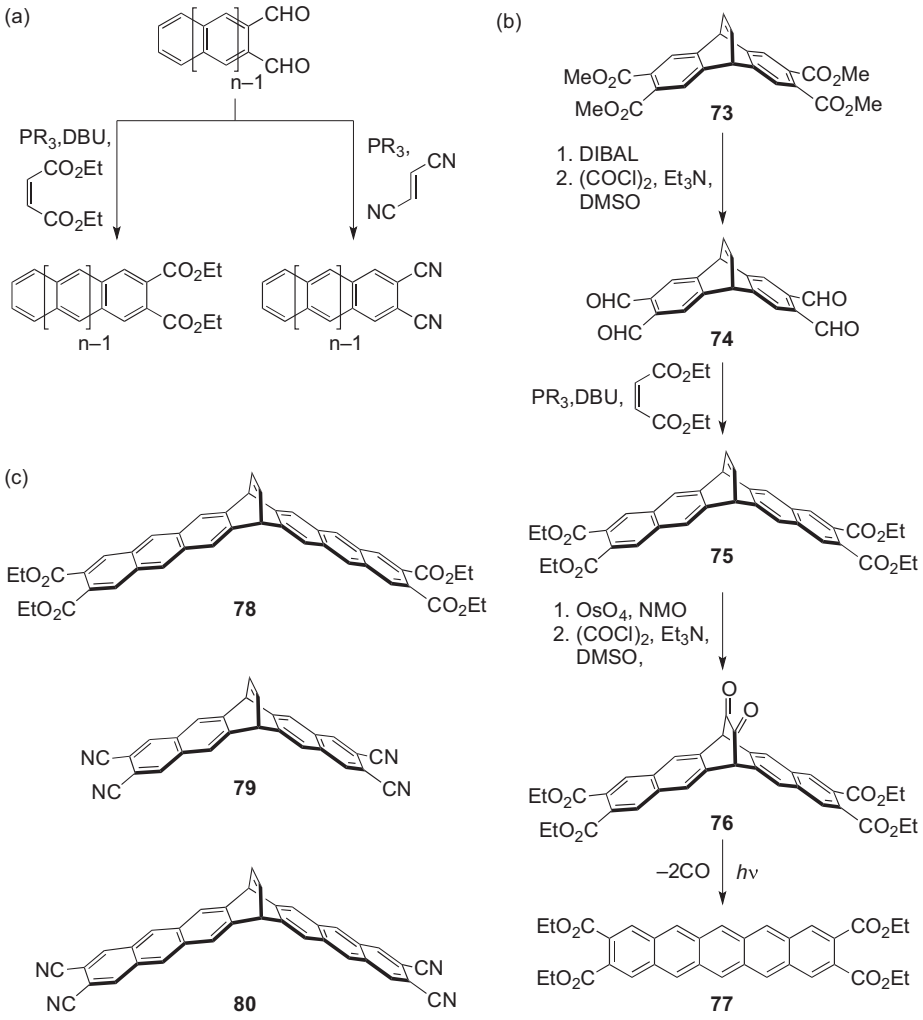

Scheme 10. Iterative synthesis of acenes via the homologation strategy reported by Lin and coworkers [74].

respectively, which dramatically increased to 0.67 and 0.70 after the photoinduced decarbonylation. The progress of the photoreaction can be monitored through change in NMR, UV, and fluorescent spectra (Fig. 8). The photoreactions of **95a** and **95b** were also possible in PMMA films.

These examples indicate the potential use of α-diketone-type acene precursors as photoswitchable fluorescent materials which could be applied in microanalysis [82], bio-imaging [83], memory media [84], etc. In contrast to reversible molecular photoswitches such as diarylethenes [85] and oxazines [86], the present system

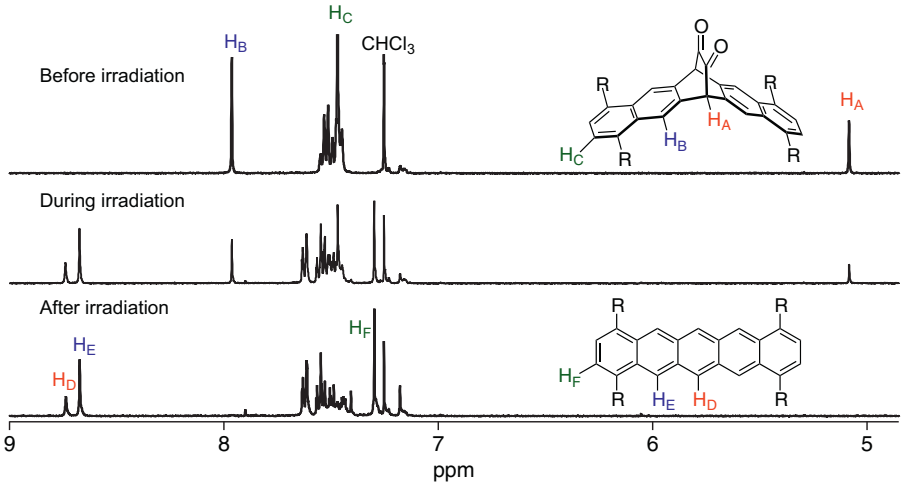

Fig. 6. Change in NMR spectra during the photolysis of **83a** in $CDCl_3$.

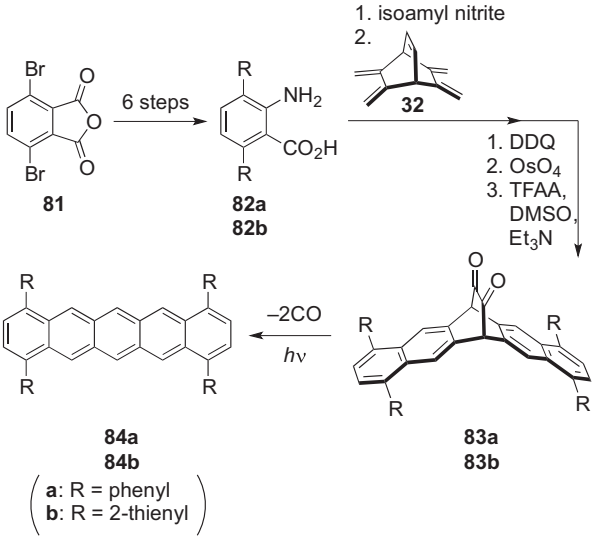

Scheme 11. Photosynthesis of 1,4,8,11-tetraaryl pentacenes **84a** and **84b** by Yamada and coworkers [75].

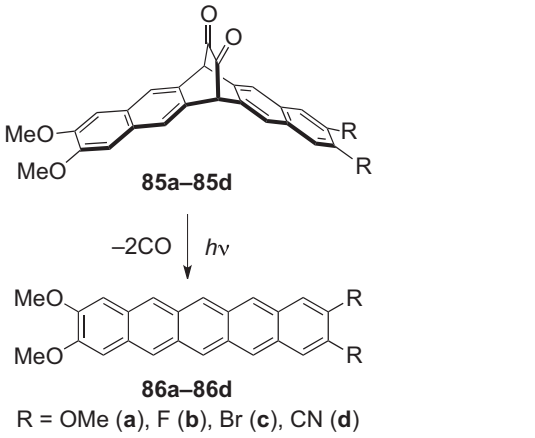

Scheme 12. Photoprecursor approach to pentacene derivatives **86a–86d** reported by Tönshoff and Bettinger [76].

Fig. 7. Photopatterned film of poly(methyl methacrylate) containing **90a**. The irradiated areas turn fluorescent because of the photoinduced conversion of non-fluorescent **90a** to highly fluorescent **91a**.

is highlighted by irreversibility of the photoreaction. Thus, α-diketone derivatives might find use especially in read-only memory media or single-molecule microscopy [87].

In 2010, Yamada et al. reported the synthesis and photochemical properties of two porphyrin derivatives fused with the α-diketone-type precursor of anthracene (**100a** and **100b**, Scheme 15) [88]. Free-base porphyrin **99a** was prepared via condensation between pyrrole **96** and diformyltripyrrane **97** followed by thermolytic removal of the ethano bridge. The corresponding palladium complex **99b** was synthesized in the same manner, except that it involved a metallation step before the thermolysis. After the Diels–Alder addition of **99a** or **99b** with vinylene carbonate, the hydrolysis–Swern oxidation sequence was carried out to afford the corresponding α-diketone derivatives **100a** or **100b**.

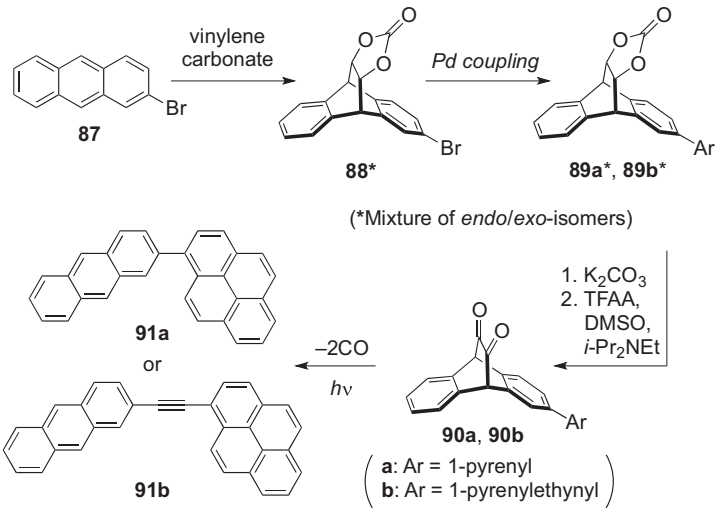

Scheme 13. Synthesis of nonfluorescent α-diketone precursors **90a** and **90b**, and their photoconversion to highly fluorescent anthracene–pyrene dyads **91a** and **91b** [77].

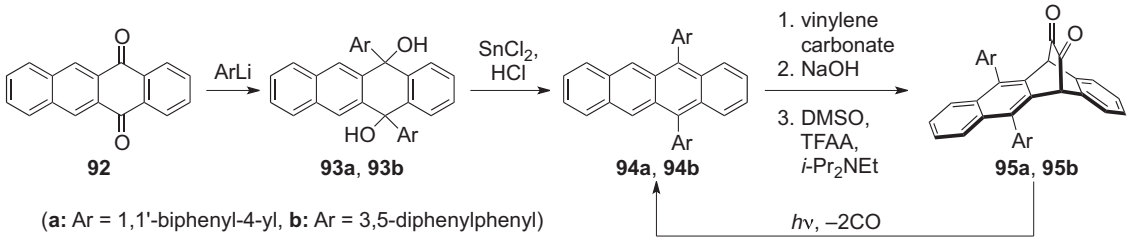

Scheme 14. Synthesis of nonfluorescent α-diketones **95a** and **95b**, and their photoconversion to highly fluorescent tetracene derivatives **94a** and **94b** [81].

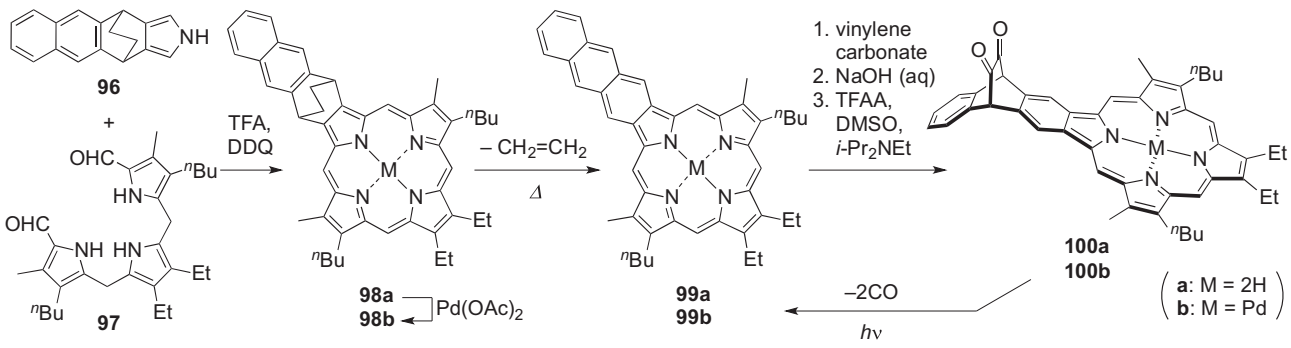

Scheme 15. Synthesis of α-diketone derivatives **100a** and **100b** reported by Yamada et al. [88].

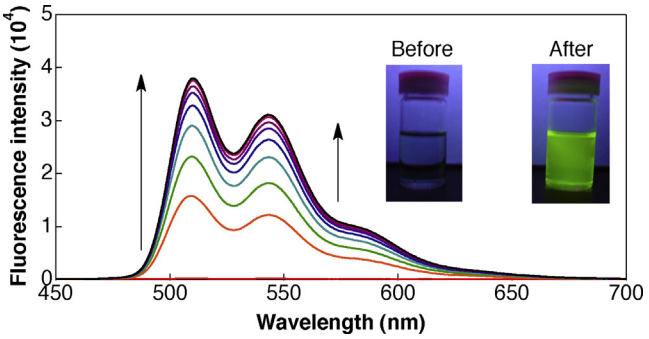

Fig. 8. Change in fluorescence spectra during photoconversion of **95a** to **94a** in a toluene solution (3.48×10^{-5} M) under argon atmosphere (λ_{ex} = 468 nm). Inset: photos of the toluene solutions before (barely fluorescent) and after (highly fluorescent) the reaction [81].

The decarbonylation reaction of **100a** and **100b** proceeded quantitatively when their Soret band was irradiated in benzonitrile solutions. Here, the n–π* absorption of the α-diketone moiety is overlapped by the much larger Soret band of the porphyrin unit, and thus direct n–π* excitation of the α-diketone unit is considered negligible during the photoreaction. The reaction quantum yields (Φ_r) in benzonitrile were calculated to be 0.029 ± 0.004% and 0.027 ± 0.003% for **100a** and **100b**, respectively (Table 1). The reaction efficiency increased considerably when toluene was used as solvent, to show Φ_r values of 0.44 ± 0.02% for **100a** and 0.54 ± 0.04% for **100b**. The authors assumed based on spectroscopic measurements and cyclic voltammetry that the lower efficiency in benzonitrile would be due to more favorable formation of the charge-separated states which decayed to the ground states through nonproductive pathways. In addition, the photolysis proceeded when the Q band of palladium complex **100b** was irradiated in toluene (Φ_r = 0.44 ± 0.02%). On the other hand, the free-base counterpart (**100a**) did not provide the corresponding photolyzed product **99a** upon irradiation of the Q band.

Although porphyrin derivatives and related phthalocyanine derivatives have already known as promising organic semiconductors [89–91], their solubility is often not high enough to be used in solution processes. In this context, introducing the α-diketone unit to already known, high performance organic semiconductors is highly beneficial, because it endows organic semiconductors of interest with higher solubility, thereby potentially allowing device fabrication based on solution techniques. Along these lines, Yamada et al. developed α-diketone-type precursors of substituted anthracenes (**101a**–**101c**, Scheme 16) [92,93].

Table 1
Reaction quantum yields (Φ_r [%]) measured for the photolysis of **100a** and **100b** in benzonitrile or toluene [88].

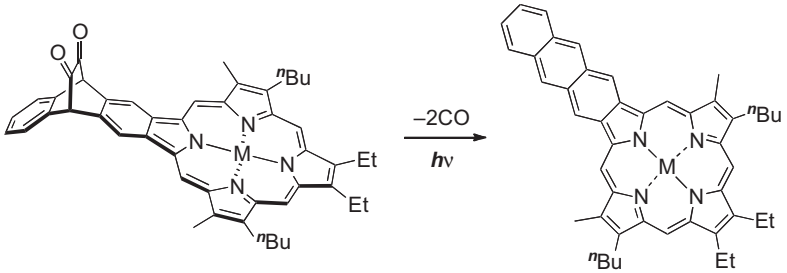

100a: (M = 2H)
100b: (M = Pd)
99a: (M = 2H)
99b: (M = Pd)

	PhCN		Toluene	
Excitation	Soret band	Q band	Soret band	Q band
100a	0.029 ± 0.004	<0.001	0.44 ± 0.02	<0.001
100b	0.027 ± 0.003	0.005 ± 0.002	0.54 ± 0.02	0.44 ± 0.02

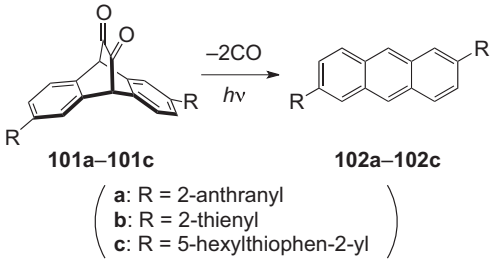

Scheme 16. α-Diketone derivatives **101a–101c** developed by Yamada and coworkers. These anthracene derivatives are soluble in common organic solvents such as chloroform and can be photolyzed to afford **102a–102c** both in solution and in the solid state [92,93].

It was successfully demonstrated that these α-diketone derivatives can be photolyzed in films to afford **102a–102c**. Performance of solution-processed devices based on these compounds will be described in Section 4.

3. Mechanism of α-diketone photolysis

The general photochemistry of α-diketones has already been well studied [53]. However, only a few studies have been reported on the mechanism of the photochemical elimination of two CO molecules from α-diketones [50,54,55,57,94]. Yamada et al. suggested in one of their early reports that the photolysis of α-diketone pentacene **37** would proceed via a singlet excited state based on their experimental observation [57]. A few years later, Neckers and coworkers carried out steady state photolysis, nanosecond laser flush photolysis, and femtosecond pump-probe experiment to understand the photolysis mechanism of the α-diketone-type precursors of anthracene (**16**), hexacene (**44**), and heptacene (**45**) [94]. Their results indicated that both the singlet and the triplet excited states would be involved in the photoinduced decarbonylation process; namely, after the excitation to a singlet excited state, the α-diketones undergo vibrational relaxation and decarbonylation from the singlet manifold, or alternatively they undergo vibrational relaxation, intersystem crossing, then decarbonylation from the triplet manifold. They also speculated that most likely the bond between a carbonyl carbon and a bridgehead carbon would break first to form a biradical species. However, they did not rule out the alternative possibility in which the bond between the two carbonyl carbons dissociates first. Bettinger et al. conducted a theoretical investigation on the photolysis mechanism of the anthracene precursor **16** based on the potential energy profiles for the ground (S_0), first singlet excited (S_1), and first triplet excited (T_1) states [54]. They carried out density functional theory (DFT) geometry optimizations, and coupled-cluster (CCSD(T)) and second-order multireference perturbation theory (MRMP2) energy estimations to map the energy profiles. These calculations indicated that the first step on the T_1 surface involves cleavage of the C–C bond between one of the bridgeheads and the neighboring carbonyl group to yield a biradical intermediate, followed by the loss of two CO molecules to give triplet anthracene. On the S_1 surface, a conical intersection of the S_1 surface with the S_0 surface exists after the transition state for the analogous C–C bond cleavage, which provides a means for relaxation to the biradical intermediate on the S_0 surface. From this intermediate, the concerted loss of two CO molecules can occur through a reaction with only a small barrier.

In the followings of this section, we will describe our recent findings from quantum chemical calculations where the photolysis paths via higher excited states were also taken into consideration. We employed the benzene precursor (**103**, Scheme 17) as a model, which is the smallest α-diketone derivative to give off an aromatic compound by decarbonylation. Here, our focus is on the singlet excited state paths, and triplet paths will not be mentioned. The results indicate that the key excited states in the photocleavage reaction are the 1^1B_1 and 1^1B_2 states. If the molecule is excited to the 1^1B_1 state, it follows a path where two CO molecules dissociate directly through a barrierless relaxation, although state crossing regions may need to be passed. If the molecule is excited to the 1^1B_2 state, it first becomes a biradical and then dissociates to benzene and ethylenedione that falls apart to two CO molecules subsequently. The reaction on the 1^1B_2 state needs a small activation energy of about 12 kcal/mol.

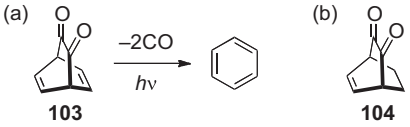

Scheme 17. (a) The model system employed in the present computational study on the mechanism of α-diketone photolysis. The starting material **103** gives off two carbon monoxide and one benzene molecules upon photoirradiation. (b) α-Diketone compound **104** studied by Rubin and Kapon [55].

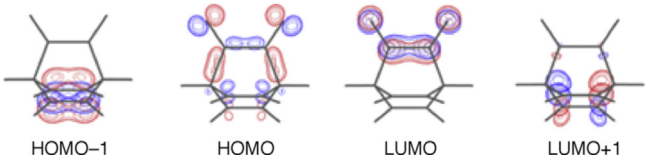

Fig. 9. RHF MOs involved in the low-lying excited states.

3.1. Mechanism of benzene diketone photolysis

Let us first discuss the electronic structures of low-lying excited states of the α-diketone-type benzene precursor (**103**). The configuration interaction singles (CIS) method and time-dependent density functional theory (TD-DFT) with the 6-31G(d) basis set were used for the calculations. Table 2 shows the excitation energies for the S_1 (1^1B_2) and selected low-lying excited states with large oscillator strength (the 2^1A_1 and 1^1B_1 states), while Fig. 9 shows the restricted Hartree–Fock (RHF) molecular orbitals (MOs) involved in the corresponding excitations. Note that the definitions of B_1 and B_2 are opposite of those in the recent work by Bettinger et al. [54].

The lowest excited state (1^1B_2) is due to the HOMO–LUMO excitation, of which energy is 3.92 and 2.67 eV in the CIS and TD-DFT methods, respectively. The oscillator strength is very small in both the methods. The 2^1A_1 and 1^1B_1 states are due to the HOMO − 1 → LUMO and HOMO → LUMO + 1 excitations, respectively. The excitation energy for the 2^1A_1 state is 7.85 and 4.71 eV in the CIS and TD-DFT methods, respectively, and that for the 1^1B_1 state is 7.62 and 4.68 eV in the CIS and TD-DFT methods, respectively. The oscillator strengths for these states are relatively large compared with the 1^1B_1 state. These three are the candidate excited states that may be involved in the photocleavage reaction. A trend can be seen in Table 2 that the excitation energies obtained by the TD-DFT method are smaller than those of the CIS method. In general, the energies of unoccupied orbitals are overestimated by the RHF method and underestimated by the DFT method. Hence, excitation energies tend to be overestimated by the CIS method and underestimated by the TD-DFT method. Since both the methods provided the same orbital pictures for each state, the CIS method was mainly used in studying the reaction on the potential energy surfaces.

Then, let us discuss the photocleavage reaction proceeding via those low-lying excited states. First, the potential energy surfaces

Table 2
Excitation energies, main configurations, and oscillator strengths of selected low-lying excited states.

Method	State	Main configuration	Excitation energy (eV)	Oscillator strength
CIS/6-31G(d)	$S_1(^1B_2)$	HOMO → LUMO	3.92	0.0012
	$S_4(^1B_1)$	HOMO → LUMO + 1	7.62	0.1379
	$S_5(^1A_1)$	HOMO − 1 → LUMO	7.85	0.1455
TD-DFT/6-31G(d)	$S_1(^1B_2)$	HOMO → LUMO	2.67	0.0013
	$S_3(^1B_1)$	HOMO → LUMO + 1	4.68	0.0099
	$S_4(^1A_1)$	HOMO − 1 → LUMO	4.71	0.0559

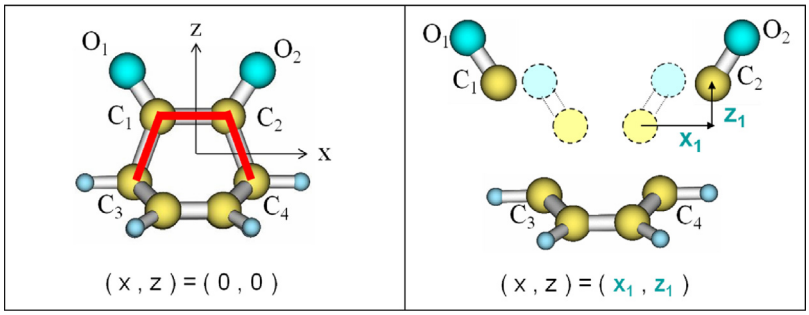

Fig. 10. Definition of the coordinate system in the examination of potential energy surfaces.

for the 2^1A_1, 1^1A_2, 1^1B_1, and 1^1B_2 states were examined with only the C_1–C_3, C_2–C_4, and C_1–C_2 bond lengths relaxed and the other geometrical parameters fixed. Here, the *x* and *z* axes were taken as in Fig. 10. The resulting potential energy surfaces (PESs) indicate that only the surface of the 1^1B_1 state has a downhill slope along the positive *x* and *z* axes, namely, the direction to the dissociation of two CO molecules. This means that the dissociation of two CO molecules can occur on the PES of the 1^1B_1 state. On the basis of these results, the 1^1B_1 state's PES taking into account of the relaxation of the cyclic part was generated, which is shown in Fig. 11.

Fig. 11 clearly shows that the PES of the 1^1B_1 state has a downhill slope (a larger gradient toward *x* than toward *z*) and suggests that the $(CO)_2$ moiety of the benzene precursor **103** is eliminated as two CO molecules directly on the 1^1B_1 surface. This suggestion can be confirmed by computing the intrinsic reaction coordinate (IRC) for the reaction: $C_6H_6(CO)_2 \rightarrow 2CO + C_6H_6$. (The IRC on the 1^1B_1 surface was obtained by starting from the ground state geometry.) The potential energies and geometries along the IRC are shown in Fig. 12, which indicates that the benzene precursor extrudes two CO molecules directly on the 1^1B_1 state, although it needs to pass through surface crossing regions to other states. It is consistent with the path indicated by the PES in Fig. 11.

Experimentally, the photolysis of α-diketone derivatives is often effected by direct irradiation of the n–π* excitation band associated with the α-diketone moiety. The corresponding absorption peaks typically locate within a range of 450–470 nm (2.6–2.8 eV) and do not vary much among different derivatives (e.g., 465 and 454 nm for pentacene derivative **37** [57] and compound **104** [55], respectively). This experimentally employed excitation energies are closer to the computed values for the 1^1B_2 state of the model compound **103** than those for the 1^1B_1 state (Table 2). Thus, it might be a reasonable assumption that the photocleavage reaction of α-diketones could also occur following the excitation to the 1^1B_2 state instead of the 1^1B_1 state. However, the PESs of the 1^1B_2 state show no negative gradient, which implies the existence of the transition state in the way to elimination of an ethylenedione molecule or two CO molecules.

To examine the photocleavage reaction in the 1^1B_2 state, we performed geometry optimization for the transition state and intermediate structures in the 1^1B_2 state. The energy diagram in Fig. 13 shows that there is a route in which the C_1–C_3 and C_2–C_4 bonds can break sequentially and ethylenedione is yielded. After the excitation to the 1^1B_2 state, the molecule runs over the TS1 of 12-kcal/mol height becoming a biradical intermediate; then it dissociates to ethylenedione and benzene via the TS2 of a lower height.

To confirm that the reaction can really proceed via this pathway, ab initio molecular dynamics (MD) simulations on the 1^1B_2 surface were carried out. Many MD trajectories with various initial geometries were taken, and not a small proportion of the

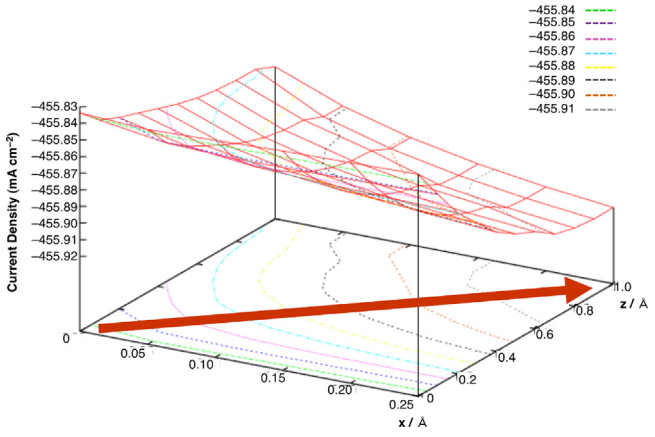

Fig. 11. Potential energy surface of the 1^1B_1 state calculated by the CIS method.

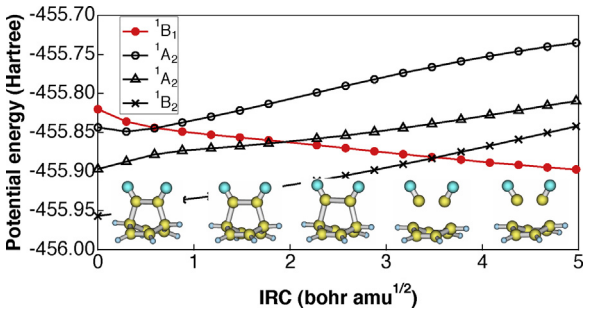

Fig. 12. Potential energies and geometries along the IRC.

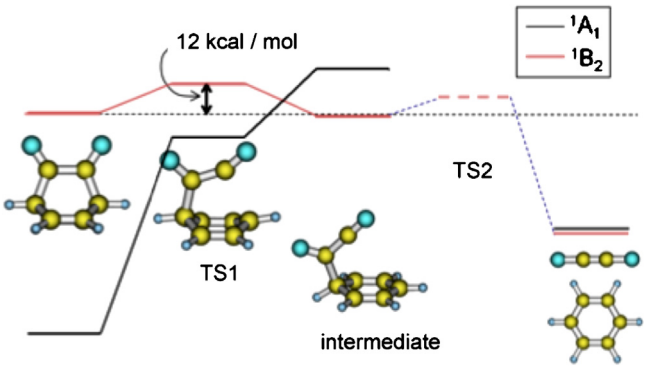

Fig. 13. Energy diagram for the reaction: $C_6H_6(CO)_2$ (**103**) → OCCO + C_6H_6.

trajectories gave ethylenedione and benzene molecules. Fig. 14 shows the change in potential energy of the 1^1B_2 state and the molecular structures along a typical trajectory. This figure clearly shows that the molecule can pass through the biradical and then dissociate into ethylenedione and benzene. It is consistent with the reaction path suggested by the analysis of transition states and intermediate structures. This result shows that the photocleavage reaction of the benzene precursor **103** can proceed on the 1^1B_2 state's PES, although a small potential barrier exists.

3.2. Mechanism of anthracene and pentacene diketone photolysis

The PESs of the anthracene and pentacene precursors **16** and **37** were also surveyed using the same methods. A feature different from the benzene precursor **103** is that the energy gaps between the excited states are rather small compared with the benzene precursor. As a result, the PES topographies of **16** and **37** are more complicated than those for **103** because of the crossing and/or avoiding crossing to other states. The results of the anthracene and pentacene precursors show that only the PESs of some $^1B_1$ states have negative gradients both toward the *z* and *x* directions. This indicates that α-diketones **16** and **37** can directly extrude two CO on the $^1B_1$ states similarly to the case of **103**. Although the experiments imply the path through the $^1B_2$ states, it has not been well clarified yet if there are dynamical paths in the $^1B_2$ states for the anthracene and pentacene precursors.

3.3. Summary on the mechanism of α-diketone photolysis

The benzene precursor **103** has two paths in the singlet states for the photocleavage reaction. One of them is the path on the PES of 1^1B_1 state. After the excitation to the 1^1B_1 state, the molecule dissociates directly into two CO molecules and benzene. The other is the path on the 1^1B_2 state. The molecule in the 1^1B_2 state passes through the biradical structure and then dissociates into ethylenedione and benzene. This path has an activation barrier. It is also found for anthracene and pentacene precursors that after the excitation to the $^1B_1$ state the photocleavage reaction can proceed via the reaction paths similar to **103**.

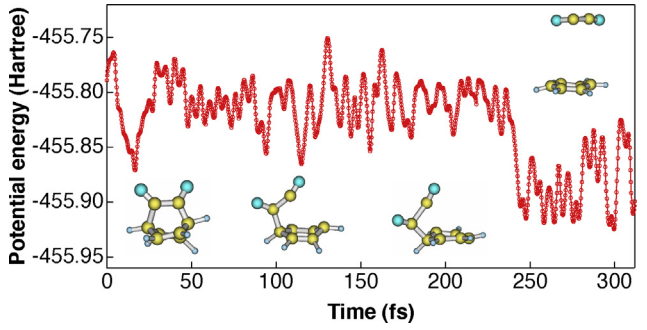

Fig. 14. Change in potential energy and molecular structure along a trajectory to ethylenedione and benzene.

4. Device fabrication by the photoprecursor method

4.1. Film preparation

As described in Sections 1 and 2, α-diketone-type precursors of acenes are generally more soluble and stable than the corresponding acene compounds. By taking advantage of these features, it is possible to fabricate acene-based thin films via solution processes even when the acene compound of interest is not compatible by itself with solution processes. Specifically, one can first deposit an α-diketone-type precursor of acene compound via a simple solution technique such as spin-coating or drop casting, then convert the precursor to the target acene compound within the film by photoirradiation under inert atmosphere. Thus obtained thin films can serve as active layers in organic (opto)electronic devices. Ideally, the photoinduced reaction is quantitative without leaving any side products in the resulting film, because the purity of the compound(s) in an active layer often has significant impact on device performance.

The progress of photoconversion reaction within films can be monitored by UV–vis and infrared (IR) spectroscopy. Fig. 15 shows absorption spectra of the thin films prepared by spin-coating of pentacene precursor **37** from a chloroform or *o*-dichlorobenzene (DCB) solution, either with or without post-deposition photoirradiation to generate pentacene (**1**). For comparison, the spectrum of a vacuum-deposited film of **1** is also presented. In the UV–vis spectra, the n–π* absorption of α-diketone moiety at 470 nm disappears upon photoirradiation, while peaks characteristic of **1** emerge (compare traces a2 and a4 in Fig. 15a). In the IR spectra, the C=O stretching peak around 1730 cm^{-1} disappears upon photoirradiation (compare traces b1 and b3 in Fig. 15b). It can be also seen in Fig. 15 that the progress of the photoconversion reaction strongly depends on the solvent used in the deposition process. Precursor **37** can be fully converted in a film prepared from a solution in DCB (boiling point 180.5 °C)—after photoirradiation, the UV–vis spectrum of the film was very similar to that of the vacuum-evaporated pentacene film (compare traces a4 and a5), and no C=O stretching was observed in the IR spectrum (trace b3). In contrast, the absorption features associated with precursor **37** remained after photoirradiation when the film was prepared from a solution in chloroform (boiling point 61.2 °C), indicating that the conversion to **1** was incomplete in this case (traces a3 and b2). These observations may be explained by an assumption that the higher boiling-point solvent (DCB) could maintain a deposited film in a semidry state during the photoconversion reaction, allowing the molecules in the film to easily reorganize so as to accommodate the structural change associated with the decarbonylation reaction (i.e., from nonplanar **37** to planar **1**). On the other hand, the lower boiling-point solvent (chloroform) might have evaporated before the reaction completed, at which point further conversion of the precursor was severely hampered because of the significantly smaller mobility allowed for molecules without solvation.

Change in surface morphology during the photoconversion of a spin-coated film of **37** (from a chlorobenzene solution) was observed by atomic force microscopy (AFM). As shown in Fig. 16, the film before photoirradiation exhibited a very smooth surface with no visible structures. Upon photoirradiation, submicrometer-sized grains emerged in places over time, which eventually covered the entire surface. This observation indicates that the as-spun film

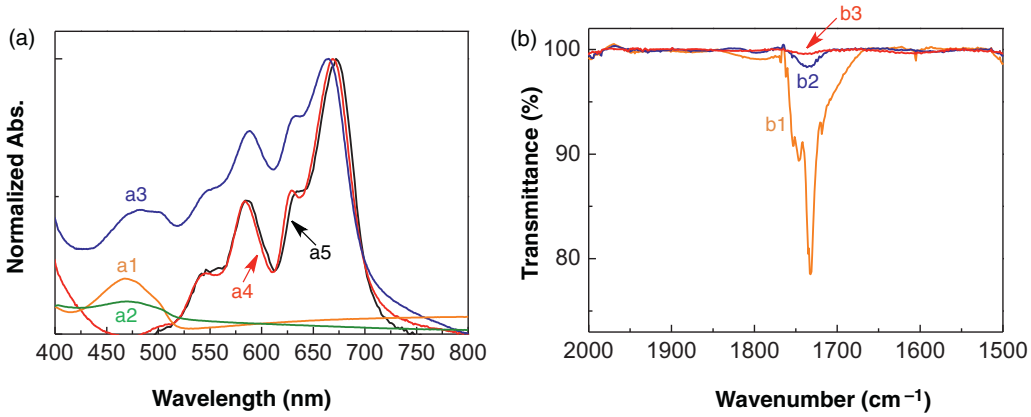

Fig. 15. (a) UV–vis spectra of thin films. (b) Attenuated total reflection-Fourier transform IR spectra of thin films. Film preparation: a1 and b1, spin-coating **37** using chloroform; a2, spin-coating **37** using DCB; a3 and b2, spin-coating **37** using chloroform then photoirradiation; a4 and b3, spin-coating **37** using DCB then photoirradiation; a5, pentacene was vacuum-evaporated [107].

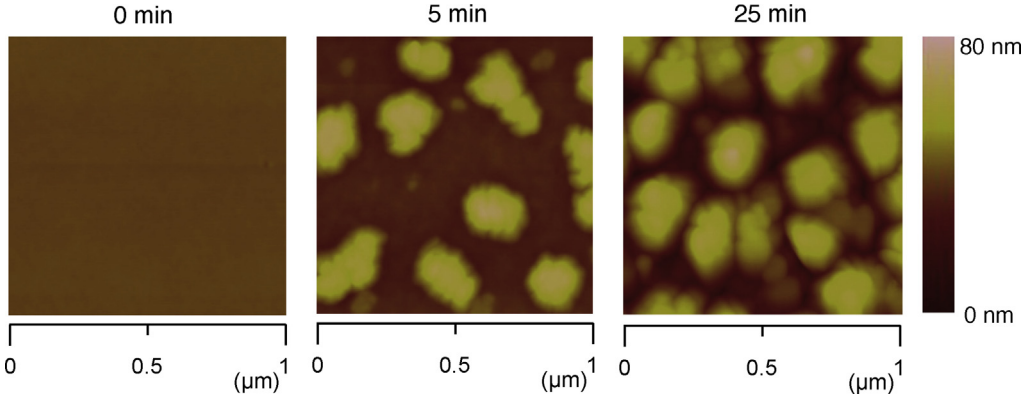

Fig. 16. AFM images of a spin-coated film of photoprecursor **37** after various photoirradiation times. The photoirradiation intensity was 200 mW cm^{-2}. Chlorobenzene was used as solvent for spin-coating.

composes of randomly oriented molecules of **37**, and the photoconversion to **1** induces local aggregation. The surface morphology of pentacene films generated by the photoprecursor method is significantly different from that of vacuum-evaporated pentacene films having rigid dendrite structures [95]. This deviation in morphology was presumed to originate from the different film formation processes; i.e., molecular diffusion on a substrate with kinetic energy for the vacuum deposition versus molecular aggregation in a semidry state for the photoprecursor method.

A different morphology resulted when a pentacene film was prepared by drop casting of a DCB solution of precursor **37** [96]. Upon photoirradiation, a light-yellow dropped solution first turned red indicating the formation of pentacene, then changed to purple associated with the precipitation of the product **1**. As shown in Fig. 17, a thus prepared film composes of plate-like microcrystals having a size of several microns. Here, the high-boiling point (and thus slow evaporation rate) of DCB allowed the photogenerated pentacene to crystallize from the solution phase to yield a highly crystalline film.

Crystallinity of the photogenerated pentacene films prepared by spin-coating and drop casting were investigated by X-ray diffractometry (XRD) in comparison with a vacuum-deposited pentacene film (Fig. 18). The vacuum-deposited film showed a strong and sharp peak at 5.72° (d = 15.5 Å) and higher order diffraction peaks assigned to the (0 0 1) plane, indicating high crystallinity of the film and perpendicular alignment of molecules to the substrate. The drop-cast film also showed strong diffraction peaks, but at slightly higher diffraction angles (d = 14.4 Å). It is known that pentacene films exhibit polymorphism with different

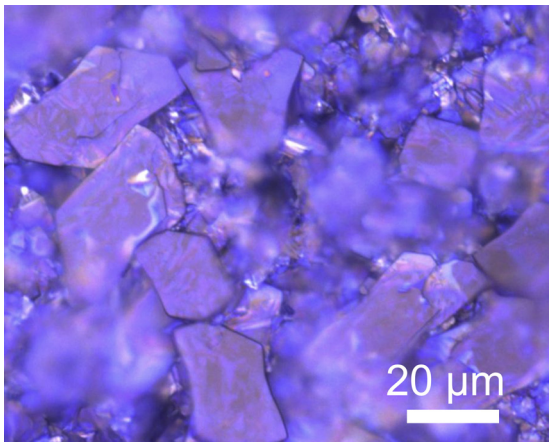

Fig. 17. An optical microscope image of a pentacene film prepared by drop casting of a DCB solution of photoprecursor **37** followed by photoinduced conversion [96].

d-spacing (d = 15.0–15.5 Å for the thin-film phase, d = 14.5 Å for the bulk phase) [97,98]. The thin-film phase has upright molecular orientation to the ab plane due to the interaction with substrate during film formation, whereas the bulk phase has slightly inclined orientation that is similar to the single-crystal structure. The XRD patterns indicate that the drop-cast film has the bulk phase, whereas the evaporated and spin-coated films have the thin-film phase. In the in-plane XRD measurements, the drop-cast film also

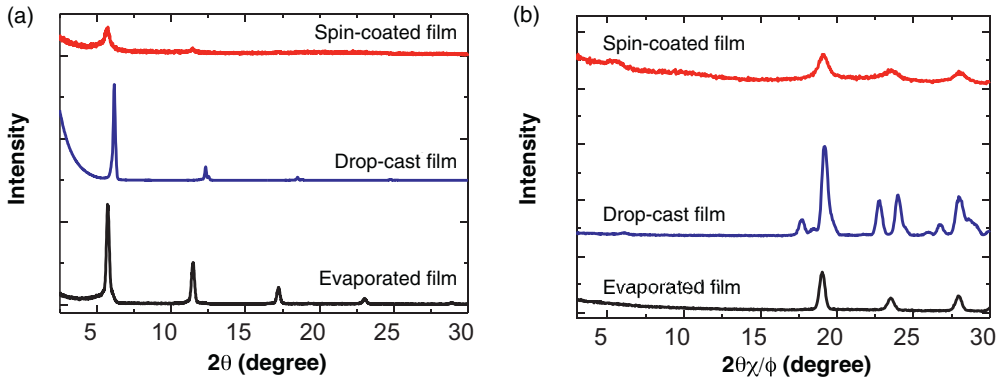

Fig. 18. X-ray diffraction patterns of pentacene films prepared by direct vacuum evaporation of pentacene (black) and by the photoprecursor method from spin-coated (red) or drop-cast (blue) photoprecursor **37**. Si/SiO_2 substrates were used for all cases. (a) Out-of-plane measurements, (b) in-plane measurements [107].

indicated bulk phase diffraction peaks at lower angles (Fig. 18b). Thus, the deposition process critically affects the resulting morphology of thin films prepared by the photoprecursor method.

4.2. Organic field-effect transistors

Organic field-effect transistors (OFETs) generally have a planar device structure composed of an organic semiconductor film, a gate insulator, and three electrodes (gate, source and drain) as shown in Fig. 19. The output current between the source and drain electrode is modulated by the gate voltage. OFETs require highly crystalline materials because the magnitude of output current is proportional to the carrier mobility of semiconductor layer. Pentacene is a traditional benchmark material for p-type OFETs, and its thin-film structure [95,97,98], electronic properties [99,100], and device performances [101–103] have been extensively studied. Pentacene has a rigid and symmetric structure with a high aspect ratio, giving highly crystalline films with the herringbone packing. In addition, vacuum-deposited pentacene tends to align vertically on the hydrophobic surface [104]. This film structure is advantageous to in-plane carrier transport, resulting in the high carrier mobility in OFET devices. Theoretical calculation predicts a longer acene gives a higher carrier mobility [105], whereas its solubility becomes lower. To obtain highly crystalline pentacene films by solution processes, several types of soluble thermo-convertible precursors have been reported as shown in Fig. 2 and Scheme 7. While some of these thermo-precursors (i.e., monoketone-type derivatives in Scheme 7) can be converted also by light, the α-diketone-type precursors can be converted only by photoirradiation. This feature would be advantageous in controlling the film structure using many parameters of light.

Bottom-gate and top-contact OFETs prepared by using α-diketone pentacene **37** have been reported [106,107]. The devices were fabricated by spin-coating a precursor solution on a pretreated substrate and subsequent photoirradiation with a blue LED lamp (Fig. 19). The source and drain gold electrodes were then thermally evaporated. In order to achieve a fair balance between the thickness and the crystallinity of resulting films, mixed solvent systems containing both low- and high-boiling-point solvents were employed in spin-coating. Fig. 20 shows typical modulation characteristics (output and transfer characteristics) of the photogenerated pentacene films prepared from spin-coated **37**. Chloroform with 1% trichlorobenzene (TCB) gave the best performance in OFET devices. The film structure and device performances were deeply affected by photoirradiation conditions. Since it is important to finish photoconversion before the spin-coated film dries up, high intensity light was suitable for obtaining higher mobility. In addition, elevated substrate temperature promoted crystallization, even though the photoconversion reaction progresses at room temperature. The optimized conditions (a light intensity of 300 mW cm^{-2}, irradiation time for 60 min, and a substrate temperature at 80 °C) yielded a carrier mobility as high as 0.86 $cm^2\,V^{-1}\,s^{-1}$ [107]. This value is one of the highest values obtained for spin-coated pentacene films, and comparable to those of vacuum-evaporated ones. It should be noted that the high carrier mobility was observed in less crystalline pentacene films showing no diffraction peaks. This anomaly may be explained by less effect of the domain boundary. The photogenerated pentacene film composes of amorphous and crystalline regions, and boundaries between crystalline domains are presumably filled by amorphous pentacene regions. As a result, more carriers can be transported to the electrodes without being trapped at domain boundaries.

In OFET materials, side alkyl chains are often employed to increase solubility and align the molecules perpendicularly on a hydrophobic surface [108]. The effect of alkyl chains in photoconvertible materials was investigated using anthracene diketone derivatives **101b** and **101c** (Scheme 16) [93]. The FET mobilities in the thin films obtained from **101b** and **101c** were estimated to be 4.7×10^{-2} and 2.6×10^{-4} $cm^2\,V^{-1}\,s^{-1}$, respectively. Thus, the compound without alkyl chains (**102b**) showed higher mobility, and this result may be explained by the different molecular arrangements observed by XRD measurements of the resulting films (Fig. 21). The film obtained from non-alkylated precursor **101b** showed a diffraction peak at $2\theta = 4.74°$ ($d = 18.6$ Å), which was assigned to the (1 0 0) plane, in the out-of-plane measurement. This indicates that molecules of **102b** aligned perpendicularly to the substrate, which is advantageous to FET carrier mobility owing to large orbital overlapping in the current flow direction [104]. In contrast, the film obtained from **101c** exhibited a very weak diffraction peak corresponding to the (0 1 1) plane in the out-of-plane measurement, indicating that molecules of **102c** partially aligned parallel to the substrate. Generally, alkyl chains in OFET materials are adsorbed on the hydrophobic surface, and align side by side during spin-coating through the van der Waals interaction. However, this type of arrangement is hardly observed for those thin films obtained by the photoprecursor method, because spin-coated precursor films are mostly amorphous, and molecular rearrangement to have alkyl chains anchored on the substrate is difficult in a solid-state film.

4.3. Organic photovoltaic cells

Organic photovoltaic (OPV) devices are based on the p–n junction similar to silicon solar cells [109], where donor molecules work as p-type semiconductor and acceptor molecules work as n-type semiconductor. Large acenes are promising materials

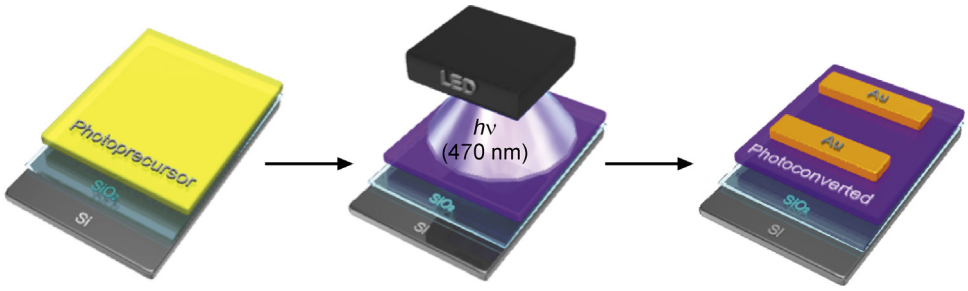

Fig. 19. Schematic illustration of the device fabrication steps for bottom-gate/top-contact type OFETs based on photogenerated organic semiconductors.

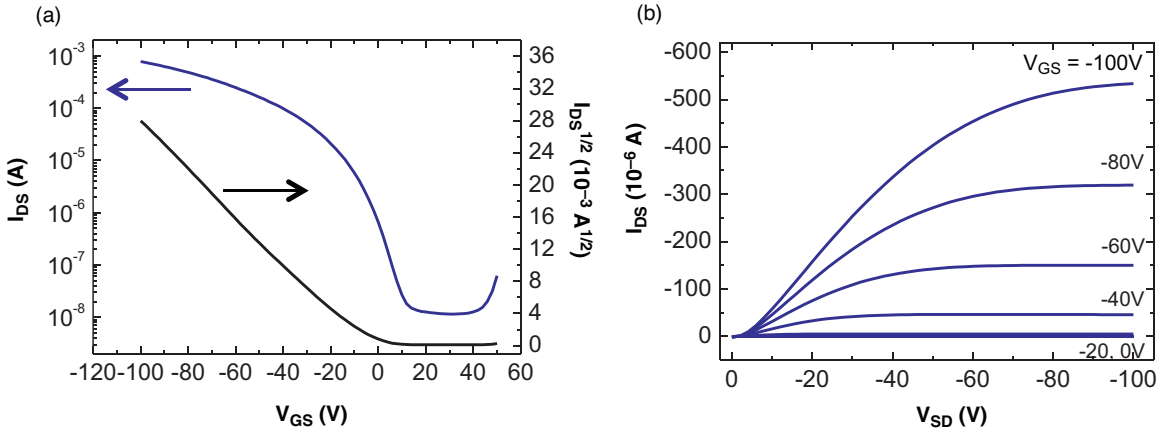

Fig. 20. Typical modulation characteristics of the OFET devices based on photogenerated pentacene films. (a) Output characteristics; (b) transfer characteristics [107].

also for photovoltaic devices due to their high carrier mobility. Indeed, high performance OPV devices using pentacene [110,111] or tetracene [112] with [60]fullerene (C_{60}) as acceptor have been reported. These acene-based p–n heterojunction devices have been mainly fabricated by vacuum deposition because of the low solubility of acenes.

Recently, pentacene films fabricated by the photoprecursor method were employed for photovoltaic devices having the p–n heterojunction structure (Fig. 22) [113]. The thin film of pentacene was prepared by spin-coating the corresponding photoprecursor **37** and subsequent photoirradiation with a blue LED lamp. An n-type layer of evaporated C_{60}/Bathocuproine (BCP) with an Al cathode or spin-coated PCBM with a Ca/Al cathode was prepared on top of the pentacene layer.

Fig. 23a shows *J*–*V* curves of the p–n junction device with evaporated C_{60} or spin-coated PCBM under AM1.5G illumination with an intensity of 100 mW cm^{-2}. Both devices exhibited the p–n diode behavior and photovoltaic response. The device with evaporated C_{60} showed PCE of 0.47% (open circuit voltage (V_{OC}) of 0.26 V, short circuit current (J_{SC}) of 3.42 mA cm^{-2}, and fill factor (FF) of 52.1%). The device with spin-coated PCBM showed PCE of 0.38% (V_{OC} = 0.47 V, J_{SC} = 1.57 mA cm^{-2}, FF = 51.1%). The higher V_{OC} of the PCBM device can be attributed to the higher LUMO level of PCBM, because V_{OC} proportionally correlates with the energy

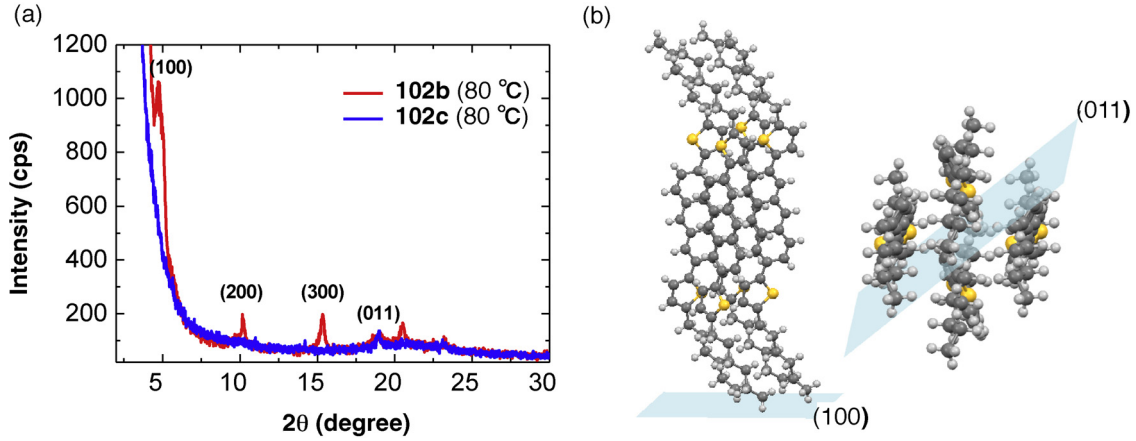

Fig. 21. (a) XRD patterns of the thin films of **102b** and **102c** prepared from the corresponding photoconvertible precursors **101b** and **101c**, respectively, on Si/SiO_2 substrates (b) (1 0 0) and (0 1 1) planes in single-crystal structure of **102c** [93].

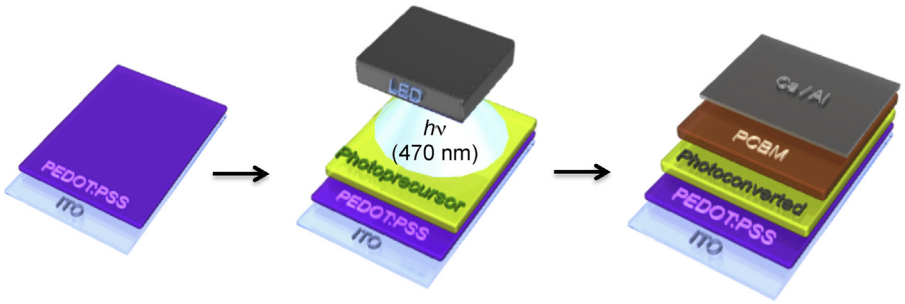

Fig. 22. Schematic illustration of the device fabrication steps for p–n heterojunction OPV devices comprising a pentacene layer prepared via the photoprecursor method.

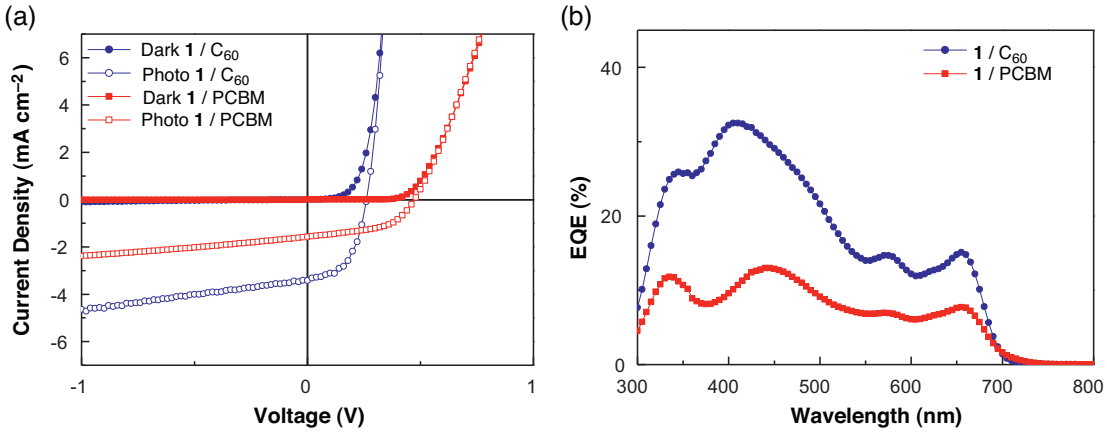

Fig. 23. Photovoltaic performances of the p–n heterojunction devices composed of the photogenerated pentacene, and the evaporated C_{60}, or the spin-coated PCBM. (a) *J–V* curves under dark condition and AM1.5G illumination. (b) External quantum efficiency (EQE) for monochromatic light.

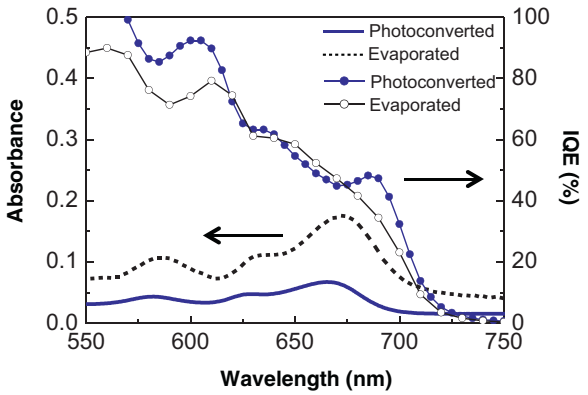

Fig. 24. UV–vis absorption and internal quantum efficiency (IQE) spectra for the p–n heterojunction device composed of photogenerated or evaporated pentacene film and fullerene C_{60} [113].

difference between the HOMO level of donor and the LUMO level of acceptor [114,115]. The external quantum efficiency (EQE) spectra (Fig. 23b) indicate that both devices have sensitivity at the pentacene absorption band around 680 nm. The J_{SC} values of the devices having a photogenerated pentacene layer are lower compared to that of a vacuum-deposited pentacene device with the configuration of ITO/pentacene/C_{60}/BCP/Al (PCE = 1.00%, V_{OC} = 0.32 V, J_{SC} = 6.32 mA cm^{-2}, FF = 49.8%). This difference is primary attributed to small thickness of the photogenerated pentacene film. Indeed, the internal quantum efficiency (IQE) of the photogenerated pentacene device was similar to that of the vacuum-deposited device (Fig. 24), indicating that the photoconverted pentacene film has equivalent potential to the vacuum-deposited film.

5. Summary and concluding remarks

This review overviewed the development of α-diketone-type precursors of acenes. α-Diketone derivatives are generally more soluble and thermally more stable than the corresponding acenes, and the α-diketone unit can be quantitatively removed by photoirradiation both in solution and in the solid state. The so-far demonstrated utility of this class of acene precursors can be categorized into three main types. The first is to provide convenient access to large or highly functionalized acenes which are otherwise difficult, if not impossible, to synthesize. The synthesis of highly unstable nonacene from an α-diketone-type precursor should be highlighted in this context [64]. In the second type of cases, α-diketone derivatives are employed as photoresponsive switches to alter optoelectronic properties of chromophores. Specifically, the α-diketone moiety is introduced as a fluorescence-quenching unit to form "masked" fluorophores, which can be "unmasked" upon photoirradiation via the photoinduced decarbonylation to retrieve the original fluorescent nature [77,81]. Such systems may find use as fluorescent molecular probes or in non-rewritable memory devices. In the third type of cases, α-diketone derivatives are used in the fabrication of acene-based organic devices by solution-based deposition techniques. The use of photoconvertible precursors is highly beneficial when the original acene compound is too insoluble or unstable to be directly employed in solution deposition. Importantly, this photoprecursor method does not require high temperature, and thus would be compatible with thermolabile substrates such as plastic. Successful application of this method to the fabrication of organic transistors and solar cells has been demonstrated [93,106,113].

As can be seen by these examples, the usefulness of α-diketone-type acene precursors was quickly recognized by the scientific community during the last decade, and their use now extends well

beyond the synthesis of large acenes. For further development of this emerging class of compounds, deeper understanding about photochemical properties and photoreaction mechanisms of a wider variety of derivatives would be essential. We believe that combined efforts among synthetic, computational, analytical, and engineering scientists would lead to effective use of photoconvertible acene precursors in technologically relevant and cost-effective ways. In this context, application of the photoprecursor method to the fabrication of organic (opto)electronic devices is highly promising.

Acknowledgments

The authors thank Prof. Noboru Ono, Prof. Hidemitsu Uno, and Dr. Yuko Yamashita in Ehime University, Dr. Daiki Kuzuhara, Dr. Shinya Ikeda, and Dr. Shuhei Katsuta in Nara Institute of Science and Technology, Dr. Takao Motoyama and Ms. Chika Ohashi in Yamagata University, and many other colleagues and students who collaborated with the authors in the project. This work was partly supported by Grants-in-Aid for Scientific Research (No. 22350083 for HY and KN and 25288092 for HY) and the Green Photonics Project in NAIST supported by MEXT, and by PRESTO, JST for HY and KN.

References

[1] S.R. Forrest, Nature 428 (2004) 911–918.
[2] H. Sirringhaus, Adv. Mater. 17 (2005) 2411–2425.
[3] M. Helgesen, R. Søndergaard, F.C. Krebs, J. Mater. Chem. 20 (2010) 36–60.
[4] F.C. Krebs, S.A. Gevorgyan, J. Alstrup, J. Mater. Chem. 19 (2009) 5442–5451.
[5] W. Cai, X. Gong, Y. Cao, Sol. Energy Mater. Sol. Cells 94 (2010) 114–127.
[6] Y. Li, Q. Guo, Z. Li, J. Pei, W. Tian, Energy Environ. Sci. 3 (2010) 1427–1436.
[7] A.J. Moulé, Curr. Opin. Solid State Mater. Sci. 14 (2010) 123–130.
[8] J. Xue, Polym. Rev. 50 (2010) 411–419.
[9] P.-L.T. Boudreault, A. Najari, M. Leclerc, Chem. Mater. 23 (2011) 456–469.
[10] B. Walker, C. Kim, T.-Q. Nguyen, Chem. Mater. 23 (2011) 470–482.
[11] C. Zhong, C. Duan, F. Huang, H. Wu, Y. Cao, Chem. Mater. 23 (2011) 326–340.
[12] X.-H. Zhu, J. Peng, Y. Cao, J. Roncali, Chem. Soc. Rev. 40 (2011) 3509–3524.
[13] S. Kola, J. Sinha, H.E. Katz, J. Polym. Sci. Part B Polym. Phys. 50 (2012) 1090–1120.
[14] X. Liu, Y.-Z. Long, L. Liao, X. Duan, Z. Fan, ACS Nano 6 (2012) 1888–1900.
[15] A. Mishra, P. Bäuerle, Angew. Chem. Int. Ed. 51 (2012) 2020–2067.
[16] P.F. Moonen, I. Yakimets, J. Huskens, Adv. Mater. 24 (2012) 5526–5541.
[17] J.D. Myers, J. Xue, Polym. Rev. 52 (2012) 1–37.
[18] R. Po, C. Carbonera, A. Bernardi, F. Tinti, N. Camaioni, Sol. Energy Mater. Sol. Cells 100 (2012) 97–114.
[19] Y. Yang, K. Mielczarek, M. Aryal, A. Zakhidov, W. Hu, ACS Nano 6 (2012) 2877–2892.
[20] R.R. Søndergaard, M. Hösel, F.C. Krebs, J. Polym. Sci. Part B Polym. Phys. 51 (2013) 16–34.
[21] A. Facchetti, Nat. Mater. 12 (2013) 598–600.
[22] J.E. Anthony, Chem. Rev. 106 (2006) 5028–5048.
[23] J.E. Anthony, Angew. Chem. Int. Ed. 47 (2008) 452–483.
[24] D. Lehnherr, R.R. Tykwinski, Materials 3 (2010) 2772–2800.
[25] R. Rieger, K. Müllen, J. Phys. Org. Chem. 23 (2010) 315–325.
[26] Y. Takeyama, S. Ono, Y. Matsumoto, Appl. Phys. Lett. 101 (2012) 083303-1–083303-4.
[27] S.S. Zade, M. Bendikov, J. Phys. Org. Chem. 25 (2012) 452–461.
[28] J.E. Anthony, J.S. Brooks, D.L. Eaton, S.R. Parkin, J. Am. Chem. Soc. 123 (2001) 9482–9483.
[29] Y. Diao, B.C.-K. Tee, G. Giri, J. Xu, D.H. Kim, H.A. Becerril, R.M. Stoltenberg, T.H. Lee, G. Xue, S.C.B. Mannsfeld, Z. Bao, Nat. Mater. 12 (2013) 665–671.
[30] L. Han, P. Mandlik, K.H. Cherenack, S. Wagner, Appl. Phys. Lett. 94 (2009) 162105-1–162105-3.
[31] M. Watanabe, K.-Y. Chen, Y.J. Chang, T.J. Chow, Acc. Chem. Res. 46 (2013) 1606–1615.
[32] A.R. Brown, A. Pomp, D.M. de Leeuw, D.B.M. Klaassen, E.E. Havinga, P. Herwig, K. Müllen, J. Appl. Phys. 79 (1996) 2136–2138.
[33] A. Afzali, C.D. Dimitrakopoulos, T.L. Breen, J. Am. Chem. Soc. 124 (2002) 8812–8813.
[34] A. Afzali, C.D. Dimitrakopoulos, T.O. Graham, Adv. Mater. 15 (2003) 2066–2069.
[35] M.-J. Joung, J.-H. Ahn, S.-Y. Kang, K.-H. Baek, S.-D. Ahn, L.-M. Do, C.-A. Kim, G.-H. Kim, I.-K. You, S.-M. Yoon, K.-S. Suh, Bull. Korean Chem. Soc. 24 (2003) 1862–1864.
[36] N. Vets, M. Smet, W. Dehaen, Tetrahedron Lett. 45 (2004) 7287–7289.
[37] K.P. Weidkamp, A. Afzali, R.M. Tromp, R.J. Hamers, J. Am. Chem. Soc. 126 (2004) 12740–12741.
[38] H.-H. Huang, H.-H. Hsieh, C.-C. Wu, C.-C. Lin, P.-T. Chou, T.-H. Chuang, Y.-S. Wen, T.J. Chow, Tetrahedron Lett. 49 (2008) 4494–4497.
[39] T.-H. Chao, M.-J. Chang, M. Watanabe, M.-H. Luo, Y.J. Chang, T.-C. Fang, K.-Y. Chen, T.J. Chow, Chem. Commun. 48 (2012) 6148–6150.
[40] M. Watanabe, W.-T. Su, K.-Y. Chen, C.-T. Chien, T.-H. Chao, Y.J. Chang, S.-W. Lin, T.J. Chow, Chem. Commun. 49 (2013) 2240–2242.
[41] K.-Y. Chen, H.-H. Hsieh, C.-C. Wu, J.-J. Hwang, T.J. Chow, Chem. Commun. (2007) 1065–1067.
[42] T.-H. Chuang, H.-H. Hsieh, C.-K. Chen, C.-C. Wu, C.-C. Lin, P.-T. Chou, T.-H. Chao, T.J. Chow, Org. Lett. 10 (2008) 2869–2872.
[43] M. Watanabe, T.-H. Chao, S.-W. Liu, C.-T. Chien, Y.J. Chang, C.-H. Yuan, K.-C. Huang, S.-H. Chien, T. Shinmyozu, T.J. Chow, J. Mater. Chem. 21 (2011) 11317–11322.
[44] C.-T. Chien, C.-C. Lin, M. Watanabe, Y.-D. Lin, T.-H. Chao, T. Chiang, X.-H. Huang, Y.-S. Wen, C.-H. Tu, C.-H. Sun, T.J. Chow, J. Mater. Chem. 22 (2012) 13070–13075.
[45] M. Watanabe, Y.J. Chang, S.-W. Liu, T.-H. Chao, K. Goto, M.M. Islam, C.-H. Yuan, Y.-T. Tao, T. Shinmyozu, T.J. Chow, Nat. Chem. 4 (2012) 574–578.
[46] M. Watanabe, T.-H. Chao, C.-T. Chien, S.-W. Liu, Y.J. Chang, K.-Y. Chen, T.J. Chow, Tetrahedron Lett. 53 (2012) 2284–2287.
[47] C.-T. Chien, T.-C. Chiang, M. Watanabe, T.-H. Chao, Y.J. Chang, Y.-D. Lin, H.-K. Lee, C.-H. Tu, C.-H. Sun, T.J. Chow, Tetrahedron Lett. 54 (2013) 903–906.
[48] D. Bryce-Smith, A. Gilbert, Chem. Commun. Lond. (1968) 1319–1320.
[49] C.F.H. Allen, Chem. Rev. 37 (1945) 209–268.
[50] J. Strating, B. Zwanenburg, A. Wagenaar, A.C. Udding, Tetrahedron Lett. 10 (1969) 125–128.
[51] J.L. Pyle, A.A. Shaffer, J.S. Cantrell, J. Org. Chem. 46 (1981) 115–118.
[52] A. Thomas, G. Anilkumar, V. Nair, Tetrahedron 52 (1996) 2481–2488.
[53] M.B. Rubin, Recent photochemistry of α-diketones, in: Photochem. Org. Synth., Springer, Berlin Heidelberg, 1985, pp. 1–56.
[54] H.F. Bettinger, R. Mondal, M. Krasowska, D.C. Neckers, J. Org. Chem. 78 (2013) 1851–1857.
[55] M.B. Rubin, M. Kapon, J. Photochem. Photobiol. Chem. 124 (1999) 41–46.
[56] H. Uno, Y. Yamashita, M. Kikuchi, H. Watanabe, H. Yamada, T. Okujima, T. Ogawa, N. Ono, Tetrahedron Lett. 46 (2005) 1981–1983.
[57] H. Yamada, Y. Yamashita, M. Kikuchi, H. Watanabe, T. Okujima, H. Uno, T. Ogawa, K. Ohara, N. Ono, Chem. Eur. J. 11 (2005) 6212–6220.
[58] T. Aotake, S. Ikeda, D. Kuzuhara, S. Mori, T. Okujima, H. Uno, H. Yamada, Eur. J. Org. Chem. 2012 (2012) 1723–1729.
[59] Y. Kamura, I. Shirotani, H. Inokuchi, Y. Maruyama, Chem. Lett. 3 (1974) 627–630.
[60] R. Mondal, R.M. Adhikari, B.K. Shah, D.C. Neckers, Org. Lett. 9 (2007) 2505–2508.
[61] R. Mondal, C. Tönshoff, D. Khon, D.C. Neckers, H.F. Bettinger, J. Am. Chem. Soc. 131 (2009) 14281–14289.
[62] H.F. Bettinger, R. Mondal, D.C. Neckers, Chem. Commun. (2007) 5209–5211.
[63] R. Mondal, B.K. Shah, D.C. Neckers, J. Photochem. Photobiol. Chem. 192 (2007) 36–40.
[64] C. Tönshoff, H.F. Bettinger, Angew. Chem. Int. Ed. 49 (2010) 4125–4128.
[65] D.R. Maulding, B.G. Roberts, J. Org. Chem. 34 (1969) 1734–1736.
[66] C.F.H. Allen, A. Bell, J. Am. Chem. Soc. 64 (1942) 1253–1260.
[67] A. Mallouli, Y. Lepage, Synthesis 9 (1980) 689.
[68] T. Takahashi, M. Kitamura, B. Shen, K. Nakajima, J. Am. Chem. Soc. 122 (2000) 12876–12877.
[69] D.M. Bowles, J.E. Anthony, Org. Lett. 2 (2000) 85–87.
[70] T. Takahashi, S. Li, W. Huang, F. Kong, K. Nakajima, B. Shen, T. Ohe, K. Kanno, J. Org. Chem. 71 (2006) 7967–7977.
[71] M.T. Stone, H.L. Anderson, J. Org. Chem. 72 (2007) 9776–9778.
[72] Y. Zhao, R. Mondal, D.C. Neckers, J. Org. Chem. 73 (2008) 5506–5513.
[73] Y. Zhao, X. Cai, E. Danilov, G. Li, D.C. Neckers, Photochem. Photobiol. Sci. 8 (2009) 34–36.
[74] C.-H. Lin, K.-H. Lin, B. Pal, L.-D. Tsou, Chem. Commun. (2009) 803–805.
[75] S. Katsuta, H. Yamada, T. Okujima, H. Uno, Tetrahedron Lett. 51 (2010) 1397–1400.
[76] C. Tönshoff, H.F. Bettinger, Chem. Eur. J. 18 (2012) 1789–1799.
[77] T. Aotake, H. Tanimoto, H. Hotta, D. Kuzuhara, T. Okujima, H. Uno, H. Yamada, Chem. Commun. 49 (2013) 3661–3663.
[78] M. Baumgarten, L. Gherghel, J. Friedrich, M. Jurczok, W. Rettig, J. Phys. Chem. A 104 (2000) 1130–1140.
[79] W. Weigel, W. Rettig, M. Dekhtyar, C. Modrakowski, M. Beinhoff, A.D. Schlüter, J. Phys. Chem. A 107 (2003) 5941–5947.
[80] S.-W. Yang, A. Elangovan, K.-C. Hwang, T.-I. Ho, J. Phys. Chem. B 109 (2005) 16628–16635.
[81] T. Aotake, Y. Yamashita, T. Okujima, N. Shirasawa, Y. Jo, S. Fujimori, H. Uno, N. Ono, H. Yamada, Tetrahedron Lett. 54 (2013) 1790–1793.
[82] W.E. Moerner, J. Phys. Chem. B 106 (2002) 910–927.
[83] M. Vendrell, D. Zhai, J.C. Er, Y.-T. Chang, Chem. Rev. 112 (2012) 4391–4420.
[84] S. Kawata, Y. Kawata, Chem. Rev. 100 (2000) 1777–1788.
[85] M. Irie, T. Fukaminato, T. Sasaki, N. Tamai, T. Kawai, Nature 420 (2002) 759–760.
[86] E. Deniz, S. Sortino, F.M. Raymo, J. Phys. Chem. Lett. 1 (2010) 1690–1693.
[87] D.W. Pohl, W. Denk, M. Lanz, Appl. Phys. Lett. 44 (1984) 651–653.
[88] H. Yamada, D. Kuzuhara, K. Ohkubo, T. Takahashi, T. Okujima, H. Uno, N. Ono, S. Fukuzumi, J. Mater. Chem. 20 (2010) 3011–3024.

[89] K. Kadish, K.M. Smith (Eds.), The Porphyrin Handbook, Academic Press, Amsterdam, 2003.
[90] Z. Bao, A.J. Lovinger, A. Dodabalapur, Adv. Mater. 9 (1997) 42–44.
[91] J. Zhang, J. Wang, H. Wang, D. Yan, Appl. Phys. Lett. 84 (2004) 142–144.
[92] H. Yamada, E. Kawamura, S. Sakamoto, Y. Yamashita, T. Okujima, H. Uno, N. Ono, Tetrahedron Lett. 47 (2006) 7501–7504.
[93] H. Yamada, C. Ohashi, T. Aotake, S. Katsuta, Y. Honsho, H. Kawano, T. Okujima, H. Uno, N. Ono, S. Seki, K. Nakayama, Chem. Commun. 48 (2012) 11136–11138.
[94] R. Mondal, A.N. Okhrimenko, B.K. Shah, D.C. Neckers, J. Phys. Chem. B 112 (2008) 11–15.
[95] R. Ruiz, D. Choudhary, B. Nickel, T. Toccoli, K.-C. Chang, A.C. Mayer, P. Clancy, J.M. Blakely, R.L. Headrick, S. Iannotta, G.G. Malliaras, Chem. Mater. 16 (2004) 4497–4508.
[96] C. Ohashi, H. Yamada, K. Nakayama, Mol. Cryst. Liq. Cryst. 580 (2013) 103–109.
[97] C.C. Mattheus, G.A. de Wijs, R.A. de Groot, T.T.M. Palstra, J. Am. Chem. Soc. 125 (2003) 6323–6330.
[98] T. Kakudate, N. Yoshimoto, Y. Saito, Appl. Phys. Lett. 90 (2007) 081903-1–081903-3.
[99] K. Hummer, C. Ambrosch-Draxl, Phys. Rev. B 72 (2005) 205205.
[100] H. Kakuta, T. Hirahara, I. Matsuda, T. Nagao, S. Hasegawa, N. Ueno, K. Sakamoto, Phys. Rev. Lett. 98 (2007) 247601.
[101] Y.-Y. Lin, D.J. Gundlach, S.F. Nelson, T.N. Jackson, IEEE Electron Device Lett. 18 (1997) 606–608.
[102] C.D. Dimitrakopoulos, A.R. Brown, A. Pomp, J. Appl. Phys. 80 (1996) 2501–2508.
[103] J. Takeya, C. Goldmann, S. Haas, K.P. Pernstich, B. Ketterer, B. Batlogg, J. Appl. Phys. 94 (2003) 5800–5804.
[104] C.D. Dimitrakopoulos, P.R.L. Malenfant, Adv. Mater. 14 (2002) 99–117.
[105] W.-Q. Deng, W.A. Goddard, J. Phys. Chem. B 108 (2004) 8614–8621.
[106] A. Masumoto, Y. Yamashita, S. Go, T. Kikuchi, H. Yamada, T. Okujima, N. Ono, H. Uno, Jpn. J. Appl. Phys. 48 (2009) 051505.
[107] K. Nakayama, C. Ohashi, Y. Oikawa, H. Motoyama, H. Yamada, J. Mater. Chem. C 1 (2013) 6244–6251.
[108] M. Halik, H. Klauk, U. Zschieschang, G. Schmid, S. Ponomarenko, S. Kirchmeyer, W. Weber, Adv. Mater. 15 (2003) 917–922.
[109] J. Janata, M. Josowicz, J. Solid State Electrochem. 13 (2009) 41–49.
[110] S. Yoo, B. Domercq, B. Kippelen, Appl. Phys. Lett. 85 (2004) 5427–5429.
[111] A.K. Pandey, J.-M. Nunzi, Appl. Phys. Lett. 89 (2006) 213506-1–213506-3.
[112] C.-W. Chu, Y. Shao, V. Shrotriya, Y. Yang, Appl. Phys. Lett. 86 (2005) 243506-1–243506-3.
[113] T. Motoyama, T. Kiyota, H. Yamada, K. Nakayama, Sol. Energy Mater. Sol. Cells 114 (2013) 156–160.
[114] M.C. Scharber, D. Mühlbacher, M. Koppe, P. Denk, C. Waldauf, A.J. Heeger, C.J. Brabec, Adv. Mater. 18 (2006) 789–794.
[115] B.P. Rand, D.P. Burk, S.R. Forrest, Phys. Rev. B 75 (2007) 115327-1–115327-11.